An ESR Study of Anisotropic Rotational Reorientation and Slow Tumbling in Liquid and Frozen Media*

S. A. GOLDMAN,† G. V. BRUNO, C. F. POLNASZEK,‡ AND J. H. FREED
Department of Chemistry, Cornell University, Ithaca, New York 14850

(Received 11 August 1971)

A careful study is described of the ESR lineshapes for the peroxylamine disulfonate (PADS) radical dissolved in 85% glycerol solution and in frozen water and D_2O. In the frozen media, spectra characteristic of rotational correlation times τ_R ranging from 1.0×10^{-11} sec to $>10^{-6}$ sec are obtained, while the range in glycerol is from 1×10^{-10} sec to $>10^{-6}$ sec. The very rapid rotational motion in frozen water is taken to imply that PADS is rotating in a clathrate cage. The activation energies in ice and 85% glycerol are 14.7 ± 0.1 and 11.3 ± 0.1 kcal/mole, respectively, (from motional-narrowing data). The value for ice is very similar to that obtained for other rate processes in ice. The lineshapes for $\tau_R\lesssim10^{-9}$ sec are analyzed in terms of the familiar spin-relaxation theories valid in the motionally narrowed region. These results are well fitted by the model of axially symmetric rotational diffusion with the symmetry axis in the plane of the N, O, and S atoms and parallel to a line passing through the two S atoms. Diffusion about this axis is found to be 2.9 ± 1 and 4.7 ± 1 times faster for frozen water and glycerol solvent, respectively than about the other axes over a wide range of values of average $\tau_{\bar{R}}$. It was possible to obtain these results, because accurate measurements of the **g** and **A** tensors for PADS in these media could be made from the well-resolved rigid spectra at X band and 35 GHz; the intrinsic widths in D_2O are only about 1.5 G. The spectra in the slow-motional region $\tau_{\bar{R}}>10^{-9}$ sec were simulated utilizing the slow tumbling formulation of Freed, Bruno, and Polnaszek appropriately generalized to include completely asymmetric **g** and **A** tensors. The simulated spectra are found, in general, to be in quite good agreement with experimental observations. The agreement is clearly improved by introducing axially symmetric rotational diffusion, as found for the motional-narrowing region, into the simulations. Spectra are simulated for Brownian rotational diffusion as well as for simplified models of free diffusion, which includes inertial effects, and for diffusion by jumps of substantial angle. Improved agreement with experiment is found with some of these latter models. What appears to be a surprisingly small nonsecular linewidth contribution in the motional-narrowing region is briefly discussed in terms of these models.

I. INTRODUCTION

There have been recent reports[1] of ESR experiments performed on systems which exhibit slow enough rotational motion that the earlier relaxation theories[2,3] are no longer applicable. In these cases the condition that $|\mathcal{H}_1(t)|\tau_R\ll1$, required for these relaxation theories, is no longer fulfilled. Here $\mathcal{H}_1(t)$ is the rotational-dependent perturbation in the spin Hamiltonian and τ_R is the rotational correlation time. In some of these experiments the rotational motion of the free radical has been used as a probe of the nature of its molecular environment. Therefore it is important to be able to interpret the observed magnetic resonance lineshapes in terms of well understood molecular and relaxation parameters. There also has been recent work on methods for simulating magnetic resonance lineshapes in this motional region.[4–7]

Freed, Bruno, and Polnaszek[4] have developed a general approach, based on the stochastic Liouville method, which can be used to simulate magnetic resonance lineshapes for any process which involves Markoffian stochastic modulation of $\mathcal{H}_1(t)$. The major objective of this work is to demonstrate the applicability of this theory to experimentally observable systems and to show its usefulness in understanding how ESR lineshapes reflect molecular motions.

The radical used in this study was peroxylamine disulfonate (PADS), since its slow motional ESR spectra contain enough "structure" to adequately test the theory, and it is possible to accurately determine its **g** tensor and **A** hyperfine interaction tensor. Unlike other commonly used nitroxides, it has the advantage that its slow motional and rigid spectra are not inhomogeneously broadened by unresolved intramolecular proton dipolar interactions, and we found that in solvents such as frozen D_2O, it is possible to obtain narrow enough rigid-spectrum linewidths to directly measure the contributions from its **g** tensor.

The properties of dilute aqueous solutions of K_2 (PADS) have been previously studied and surprisingly rapid rotational correlation times, $\tau_R\approx3\times10^{-12}$ sec, have been found.[8–10] Due to the lack of solubility and stability of PADS, there have been few studies performed in other solvents. Two experiments of interest were performed in glycerol–H_2O solutions[11,12] where the (η/T) dependence of the linewidths of the three hyperfine components were studied. However, in that work only crude data was presented and only for viscosities where $|\mathcal{H}_1(t)|\tau_R\ll1$. In the present study, rotational motion was observed both in glycerol–H_2O solutions at reduced temperatures and in frozen H_2O and D_2O. In the latter, PADS exhibits values of τ_R that vary continuously from the rigid limit $\tau_R>10^{-6}$ sec to $\tau_R\sim10^{-11}$ sec near its melting point or a range of greater than 10^5 sec. A similarly large range of τ_R from $>10^{-6}$ to 10^{-10} sec was studied in glycerol–H_2O solutions. Thus, in both media it was possible to study and analyze the nature of molecular reorientation over a much larger range than previously available.

In the case of glycerol–H_2O solutions, the results can be compared to known viscosities, while for the case of ice solvent, the rapid reorientation sheds light on the previously observed fast motion of PADS in aqueous solution. In our analysis of these results we also carefully consider the possibility of anisotropic rotational reorientation[13] and deviations from Brownian rotational diffusion.

II. EXPERIMENTAL

A. ESR Spectrometer

X-band ESR measurements were performed with a Varian E-12 spectrometer system[14] with either 10 kHz or 100 kHz field modulation in conjunction with Varian rectangular, dual sample, or large access cylindrical cavities. The temperature was controlled by a Varian E-257 variable temperature unit to within ±0.5°C. The absolute temperature was checked at the geometric center of the cavity and found to be accurate to ±1°C. The temperature gradient over the active region of the cavity, relative to the temperature at the center, was ±0.5°C.

The 35 GHz spectra were obtained with a Varian V4561 35 GHz bridge, cylindrical cavity, and pole tips in conjunction with a Varian V4502-14 spectrometer with a 12-in. magnet. The temperature was controlled with a Varian V4240 temperature controller, with a modified gas transfer and control feedback system, so that both the cavity and sample could be cooled. The temperature was monitored with a thermocouple attached to the cavity body and was stable to ±2°C. When 35 GHz spectra are taken, it is necessary to carefully position the sample in order to minimize dispersion effects. This was done by initially adjusting the sample position, at room temperature, to symmetrize the center line of the PADS spectrum before performing experiments at lower temperatures.

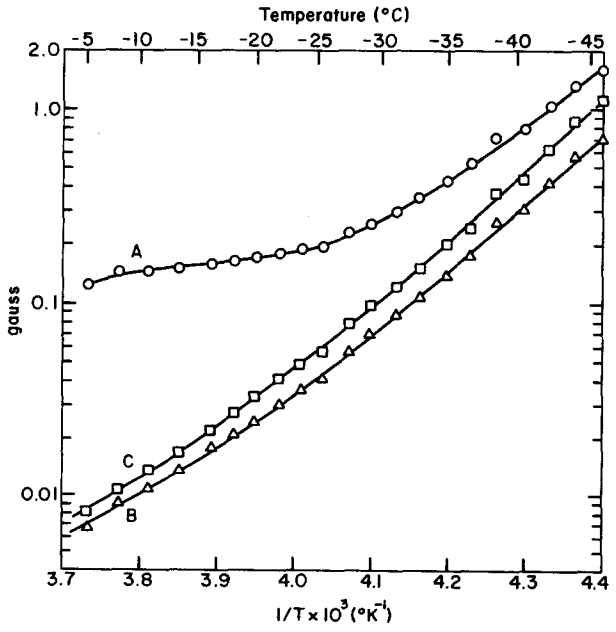

FIG. 1. *A*, *B*, and *C* versus $1/T$ for PADS in frozen H_2O.

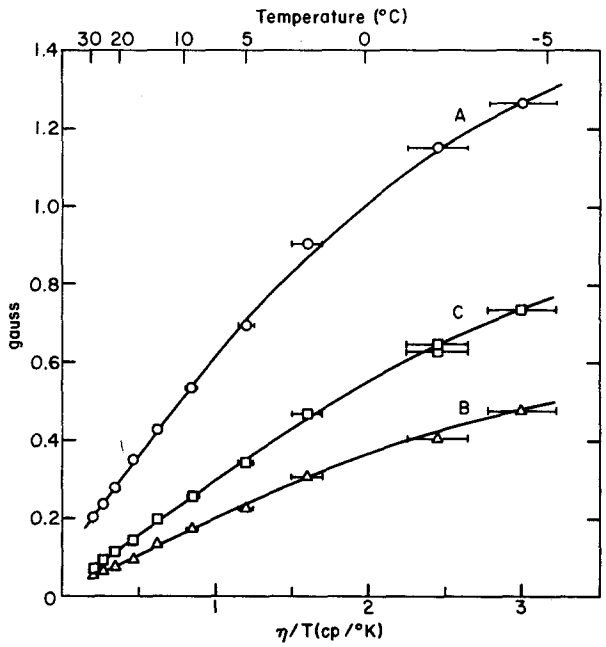

FIG. 2. *A*, *B*, and *C* versus η/T for PADS in 85% glycerol–H_2O.

The microwave frequency was measured with a Systron Donner 1037 counter with appropriate plug-in units.

B. Field Measurements

In both the X-band and 35 GHz experiments, the magnetic field sweep was calibrated with either the known splitting constants of potassium tetracyanoethylene in DME ($a_N = 1.575$ G)[15] or PADS in H_2O ($a_N = 13.091 \pm 0.004$ G).[16] For the motionally narrowed spectra, g values were measured with a dual sample cavity relative to the g value of PADS in H_2O ($g_s = 2.00550 \pm 0.00005$).[17] Suitable corrections were made for the difference in magnetic field between the two sample positions.

In the rigid-limit spectra, absolute field measurements were made in the cylindrical cavity relative to DPPH as a secondary standard. The g value of DPPH was subsequently cross-calibrated relative to the g value of PADS in H_2O. The absolute field is calculated from the measured field separations and microwave frequencies after second order corrections are made for the position of the $\bar{M} = 0$ line.[18]

C. Sample Preparation

Solutions of PADS in H_2O or D_2O (99.8%) were prepared by dissolving K_2 (PADS) in a 0.05M aqueous

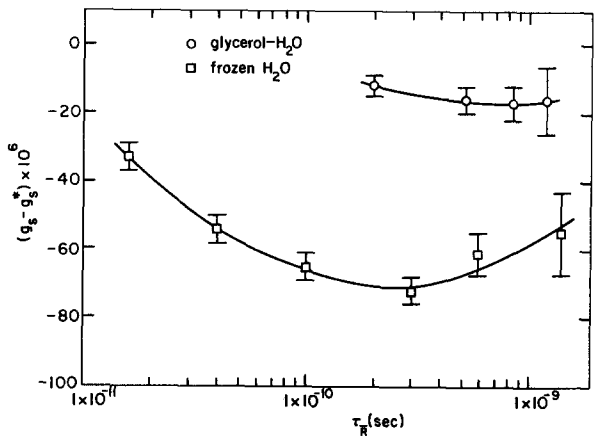

FIG. 3. g_s versus τ_R for solutions of PADS in frozen H_2O and glycerol–H_2O in the motional-narrowing region. g_s^* (PADS in H_2O, $T=+20°C$) $=2.00550\pm0.00004$. The value of g_s has been corrected for dynamic frequency shifts as described in the text.

solution of K_2CO_3. The solution was deoxygenated by bubbling with N_2 (Airco Prepurified) for at least one hour before being pipetted into sample tubes and sealed in a nitrogen atmosphere. Sample tubes were usually 3-mm o.d. Pyrex tubing except for "lossy" samples which were contained in 1- or 2-mm o.d. capillaries inserted into the 3-mm Pyrex tubing. 9-mm-o.d. and 1-mm-o.d. quartz tubes were used for the large access cylindrical cavity and 35-GHz cavity respectively.

The solutions of PADS in glycerol–H_2O were prepared by mixing measured volumes of the deoxygenated aqueous PADS solution and deoxygenated glycerol in the desired proportions. The resultant solution was cooled, further deoxygenated, and then transferred to sample tubes as previously described. These samples were stored in a freezer to prevent decomposition. The relative glycerol–H_2O concentration was determined by measuring the absolute viscosity of the mixture at $T=30.0\pm0.1°C$ and comparing the results with the known viscosity of glycerol–H_2O mixtures.[19,20] Some experiments were also performed in 100% glycerol which had been vacuum distilled to remove H_2O.

The X-band measurements on solutions of PADS in glycerol–H_2O were made on samples with low enough concentrations that there was no exchange broadening. Thus for most measurements the PADS concentration was less than $5\times10^{-4}M$. The exact concentration is uncertain, since some decomposition occurs during sample preparation and when the sample is exposed to temperatures $\gtrsim15°C$. For the 35 GHz experiment, it was necessary to use a more concentrated sample. However, it was found that in glycerol–H_2O, exchange effects are minimal in the slow motional region (high η/T).

Samples of PADS in D_2O (or H_2O) were frozen either slowly or more rapidly by immersion in liquid N_2. For very dilute samples, the spectra obtained by both methods were almost identical, but for more concentrated samples, the latter method yielded a rigid limit spectrum that had just one "exchange-broadened" line. This type of phenomenon has been noted by other authors[21] and attributed to the formation of high local concentrations of paramagnetic ions with consequent strong intermolecular exchange interactions.[22] Thus for all aqueous PADS samples, concentrations of $\lesssim1\times10^{-4}M$ were used.

III. RESULTS

A. Motional-Narrowing Results

The ESR spectrum of PADS in frozen D_2O (or H_2O) was found to vary continuously from a typical fast rotational or motional narrowing spectrum ($|\mathcal{K}_1(t)|\tau_R\ll1$) near the melting point to a rigid limit spectrum at $T\lesssim-90°C$. The motionally narrowed spectra can be described, to zero order, by the high field spin Hamiltonian

$$\hbar\mathcal{K}_0=g_s\beta_e\mathbf{S}\cdot\mathbf{B}_0-\hbar\gamma_e a_N\mathbf{I}\cdot\mathbf{S}, \tag{1}$$

where $S=\frac{1}{2}$, $I=1$, $g_s=\frac{1}{3}(g_x+g_y+g_z)$, and $a_N=\frac{1}{3}(A_x+A_y+A_z)$.

As will be shown later, the simulated slow motional spectra were found to be very sensitive to the detailed model that was assumed for the rotational motion. Considerable guidance in analyzing these spectra can be obtained by first studying the linewidth variations in the motional-narrowing region. A careful linewidth study was performed in the temperature range where $\delta\ll a_N$. Here δ is the peak-to-peak derivative linewidth. The linewidth data is expressed in terms of:

$$\delta=A+B\tilde{M}+C\tilde{M}^2, \tag{2}$$

where $\tilde{M}$ is the spectral index number.[23] The results for PADS in frozen H_2O are given in Fig. 1. The standard deviations for A, B, and C are less than 1%, 3%, and 3%, respectively, except for $T>-10°C$ where the small variation in linewidth among the three hyperfine components results in standard deviations for B and C of 4%–10%. The linewidth variations and residual width in frozen D_2O were the same as those observed in frozen H_2O except that the corresponding linewidths occurred at temperatures that were about 3°C warmer. Within experimental error, this corresponds to the 3.8°C difference between the freezing points of the two liquids.

A similar study was performed in glycerol–H_2O solutions for comparison with the studies in frozen H_2O (or D_2O). Solvents that were 85% by weight glycerol–H_2O were used in most experiments, since (1) the viscosity of this mixture has been measured as low as $-20°C$,[20] (2) the error in viscosity due to small temperature fluctuations or slight inaccuracies in sample preparation are much less than for solutions with greater glycerol content (i.e., $d\eta/dT$ and $d\eta/d\chi$, where χ is the mole fraction H_2O, are not too large), and (3) high viscosities can be achieved at reasonable tem-

peratures as compared to lower glycerol content. From our viscosity measurements, it was found that the sample preparations gave reproducible viscosities to within 1% at 30°C. This corresponds to ±0.1% reproducibility by weight. The $5\times10^{-2}M$ K_2CO_3 buffer was found to increase the viscosity of the 85% glycerol–H_2O solution by about 5%. This effect was considered small compared to the uncertainties in viscosity due to temperature fluctuations and was neglected. The results of the linewidth study for A, B, and C are given in Fig. 2 as a function of η/T.[24] The standard deviation for A, B, and C is less than 1%, 3%, and 3% respectively, except for $T\gtrsim15$°C where some sample decomposition occurs. For these temperatures, the deviation in B and C is about 10%.

The variation of g_s and a_N with τ_R was also measured for these two systems and is given in Figs. 3 and 4. These values were determined relative to those for PADS in H_2O ($T=+20$°C). Corrections have been made for dynamic frequency shifts due to time-dependent fluctuations $\mathcal{H}_1(t)$ in the Hamiltonian. Contributions from nonsecular terms have been calculated from expressions given by Fraenkel[25] corrected for anisotropic rotational diffusion as described in Sec. IV.A. These corrections, which are downfield shifts, ranged from 36 mG for values of τ_R where $\omega_0^2\tau_R^2\gg1$ ($\omega_0=5.7\times10^{10}$ sec^{-1}) to 13 mG for $\tau_R=1.6\times10^{-11}$ sec. Dynamic frequency shifts from pseudosecular terms are negligible except for values of $\tau_R\gtrsim(10\,|\,\omega_{n\pm}\,|\,)^{-1}$. However, in this region corrections due to higher order terms become important relative to the terms calculated by relaxation theory. Thus the corrections from secular and pseudosecular terms were determined from spectral simulations as described in Sec. IV.B. These corrections ranged from ~50 mG at $\tau_R=1.5\times10^{-9}$ to ~0 at $\tau_R<5\times10^{-10}$ for the $\tilde{M}=0$ line. The dynamic frequency shift from nonsecular terms does not have any significant higher order corrections for large τ_R as a consequence of the validity of high field approximations in the present work.[4]

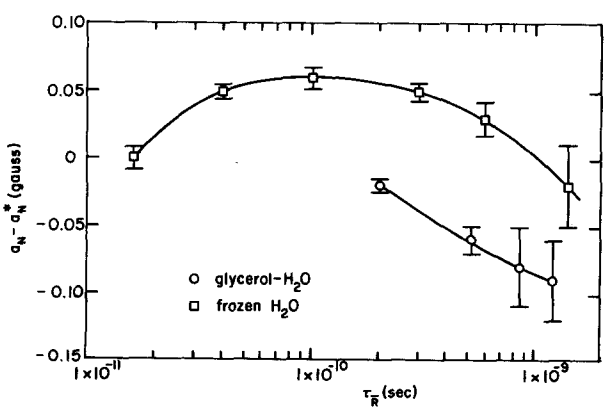

FIG. 4. a_N versus $\tau_{\tilde{R}}$ for solutions of PADS in frozen H_2O and glycerol–H_2O in the motional-narrowing region. a_N^* (PADS in H_2O, $T=+20$°C) = 13.091±0.004 G. The value of a_N has been corrected for dynamic frequency shifts as described in the text.

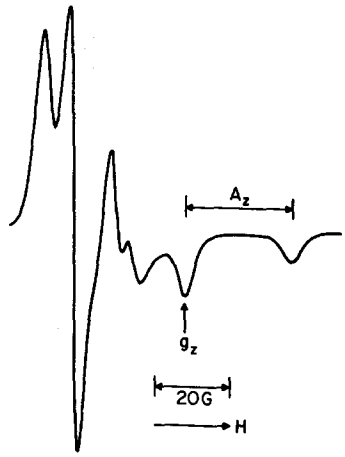

FIG. 5. 35 GHz ESR spectrum of $1\times10^{-2}M$ PADS in 85% glycerol–H_2O at $T=-70$°C.

The values for τ_R in Figs. 3 and 4 were determined directly from the measured linewidths as described in Sec. IV.A. The error limits shown include errors in estimating dynamic frequency shifts due to the small uncertainties in estimating τ_R and the molecular parameters (see next section).

After the static and dynamic frequency shift corrections were made, the corrected separations between the hyperfine lines were the same within experimental error (±10 mG).

It should be noted that the changes in g_s and a_N observed in the motional narrowing region are very small compared to the significant spectral parameters used for the line shape calculations that are discussed in the next section.

B. Simulation of Rigid-Limit Spectra

In order to simulate the spectra of PADS in both the slow motional and motional-narrowing regions, it is necessary to know the principal values of the **g** and **A** tensors. It is known from a variety of single crystal studies on nitroxides that these tensor quantities are only slightly dependent on the attached substituents and that the two tensor axes are approximately coincidental.[1a,26] While a single crystal study of PADS has been reported,[27] this data was for a different host lattice. Thus, it was necessary to determine these parameters from the available rigid spectra. In principle, this can be done by varying these six parameters and X, the residual linewidth, until the best possible fit is obtained between the simulated[28] and experimentally observed rigid spectra. However, for PADS in glycerol–H_2O, it was only possible to accurately determine A_z, g_z, and X from the X-band rigid spectra, since only the lines associated with $M=\pm1$, for orientations of the z axis parallel to the magnetic field, are well separated from the central overlapped region of the spectra. A_z is equal to one half the separation between the outer

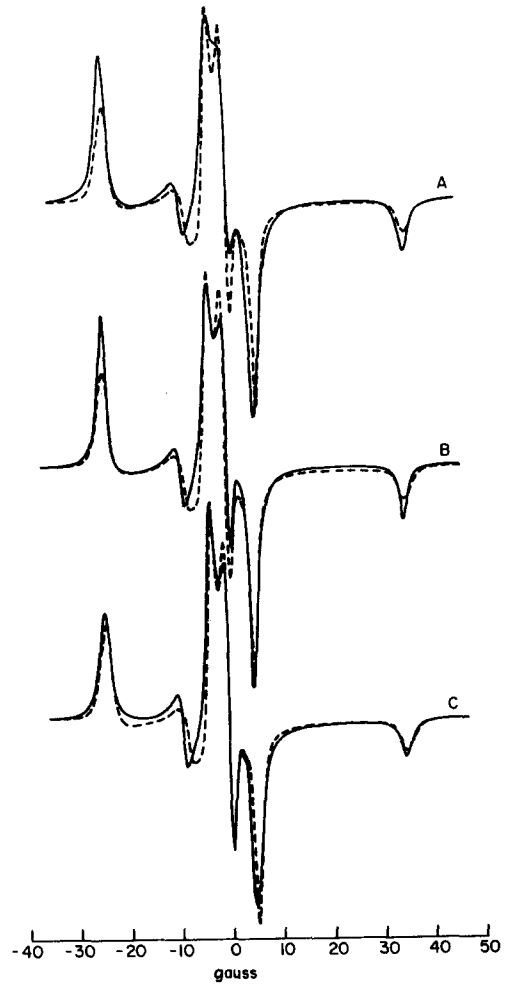

FIG. 6. Experimental and simulated X-band rigid spectra for PADS in frozen D_2O. - - -, experimental spectrum at $T=-90°C$. —, simulated rigid spectra calculated with the spectral parameters in Table I and values of α and β, in the linewidth expression given in Eq. (3), of A $\alpha=1.5$ G, $\beta=0$; B $\alpha=1.1$ G, $\beta=0$; C $\alpha=1.1$ G, $\beta=0.4$ G.

hyperfine extrema, while g_z corresponds to the midpoint of these two extrema. The residual linewidth X can be determined from the width at half height of the outer hyperfine extrema (cf, Fig. 6 for PADS in frozen D_2O).

Since the separation between the g-tensor components is proportional to B_0, rigid spectra observed at 35 GHz show greater resolution, for a given linewidth, and make accurate determination of g_x, g_y, A_x, and A_y possible. The 35 GHz spectra of PADS in both systems were obtained, but the signal to noise ratio for PADS in frozen D_2O was insufficient for detailed analysis. However, for PADS in glycerol–H_2O, comparisons between the observed (Fig. 5) and simulated rigid-limit spectra yielded the results presented in Table I. The stated errors include experimental standard deviations and an estimate of the uncertainty involved in comparing the simulated to experimental spectra. [One notes from Table I that the errors in $g^{(0)}$ and $g^{(2)}$, needed for line shape predictions, are less than the errors in the absolute values of g_x, g_y, g_z, since all simulations were performed relative to the value of g_z.]

The residual linewidth for the rigid spectrum of PADS in frozen D_2O (Fig. 6) is less than in frozen H_2O or glycerol–H_2O. The increased resolution in the central portion of the spectrum makes determination of the principal values of the **A** and **g** tensors possible from X-band simulations. The best spectral fit (Fig. 6, curve C) was obtained with the values given in Table I.

The assignment of axes in the molecular frame is based on a comparison with the single crystal results of Griffith *et al.* on di-*t*-butyl nitroxide (DTBN).[29] A comparison between the values determined for PADS with those given for DTBN (Table I) show that they are very close, and that one may safely use the same axes system for both molecules. Thus the x axis is along the N–O bond, the z axis along the $2p$–π orbital of nitrogen, with the y axis perpendicular to these.

From a detailed comparison of the simulated and experimental rigid-limit spectra, it is possible to estimate the residual Lorentzian[30] linewidth in the various systems studied. If the linewidth is determined from the width at half height of the outer hyperfine extrema, values of 1.5 ± 0.1, 2.5 ± 0.2, and 3.0 ± 0.2 G for PADS in frozen D_2O, frozen H_2O, and glycerol–H_2O, respectively, are obtained. Comparisons of spectra at X band and 35 GHz indicate that the residual linewidth for the glycerine–water solvent is field independent within the limits of experimental error. It is also evident, as shown in Fig. 6, curve A, that for PADS in frozen D_2O, it is impossible to accurately simulate the central portion of the spectrum with a linewidth of 1.5 G. A smaller linewidth of about 1.1 ± 0.1 G (Fig. 6, curve B) yields a much better fit in this region. Since the central region of the spectrum, at X band, is associated with absorptions that occur when the x and y axes are parallel to the magnetic field, it is very likely that the residual linewidth is orientation dependent.[31] Since the exact angular variation of X is unknown, we assumed the simple form

$$X=\alpha+\beta\cos^2\theta, \tag{3}$$

where θ is the polar angle. The best fit is obtained for values of α and β of 1.1 and 0.4 G, respectively, and is shown in Fig. 6, curve C. It is seen that in this case the relative amplitudes of the central region and the outer hyperfine extrema now agree with those of the experimentally observed spectra. (For PADS in glycerol–H_2O and frozen H_2O solutions, the same magnitude of orientation dependence in the linewidth is observed.[32]) Although the agreement between experimental and simulated spectra is not perfect, when one considers the fact that the expression for $X(\theta, \phi)$ is only a crude approximation and that other factors[30,33]

TABLE I. Magnetic parameters.

	PADS in frozen D_2O	PADS in 85% glycerol-H_2O	DTBN[a]	PADS[b]
g_x	2.0081±0.0002	2.00785±0.0002	2.00872±0.00005	
g_y	2.0057±0.0002	2.00590±0.0002	2.00616±0.00005	
g_z	2.0025±0.0001	2.00265±0.0001	2.00270±0.00005	
$\langle g \rangle$[c]	2.00543±0.00017	2.00547±0.00017	2.00586±0.00005	
g_s[d]	2.00545±0.00002	2.00548±0.00001		
$g^{(0)}$[e] $z'=z$	$-3.61\pm0.15\times10^{-3}$	$-3.47\pm0.13\times10^{-3}$		
$g^{(0)}$[e] $z'=y$	$3.1\pm1.5\times10^{-4}$	$5.3\pm1.4\times10^{-4}$		
$g^{(2)}$[f] $z'=z$	$1.2\pm0.1\times10^{-3}$	$9.8\pm1.0\times10^{-4}$		
$g^{(2)}$[f] $z'=y$	$-2.8\pm0.1\times10^{-3}$	$-2.6\pm0.1\times10^{-3}$		
A_x(G)	5.5±0.5	5.5±0.5	7.59±0.05	6
A_y(G)	4.0±0.5	5.0±0.5	5.95±0.05	6
A_z(G)	29.8±0.3	28.7±0.3	31.78±0.05	27
$\langle A \rangle$[g](G)	13.1±0.4	13.1±0.4	15.11±0.05	13
a_N[d](G)	13.11±0.03	13.03±0.04		
$\xi_N D^{(0)}$[h] $z'=z$	28.6±0.6	26.9±0.6		
$\xi_N D^{(0)}$[h] $z'=y$	−15.6±0.9	−13.8±0.9		
$\xi_N D^{(2)}$[i] $z'=z$	1.05±0.7	0.35±0.7		
$\xi_N D^{(2)}$[i] $z'=y$	17.0±0.6	16.2±0.6		

[a] Reference 29.
[b] Reference 27.
[c] $\langle g \rangle = \frac{1}{3}(g_x+g_y+g_z)$.
[d] Measured in motionally narrowed region. Error limits reflect total range of observed values.
[e] $g^{(0)} = (6)^{-1/2}[2g_{z'} - (g_{x'}+g_{y'})] = [3(6^{-1/2})](g_{z'}-g_s)$.
[f] $g^{(2)} = \frac{1}{2}(g_{x'}-g_{y'})$.
[g] $\langle A \rangle = \frac{1}{3}(A_x+A_y+A_z)$.
[h] $\xi_N D^{(0)} = (|\gamma_e|/2\pi)[2(6^{1/2})]^{-1}[2A_{z'}-(A_{x'}+A_{y'})]$
$= (|\gamma_e|/2\pi)[(3/2)(6^{-1/2})](A_{z'}-a_N)$ in megahertz.
[i] $\xi_N D^{(2)} = \frac{1}{4}(|\gamma_e|/2\pi)(A_{x'}-A_{y'})$ in megahertz.

which can affect the lineshape have not been considered, this agreement gives us confidence in the accuracy of the values for the **g** and **A** tensors. Since $\langle A \rangle$ and $\langle g \rangle$ are equal, within experimental error, to the isotropic values measured in the motional-narrowing region, it seems reasonable to assume that the values measured in the rigid limit can be used in the analysis of the motionally narrowed spectra.

IV. ANALYSIS AND DISCUSSION

A. Motional-Narrowing Results

In principle, it is possible to obtain an estimate of τ_R from the linewidth variations amongst the three hyperfine components of PADS. The dependence of T_2^{-1} on τ_R is given by Kooser *et al.*[8] This expression includes the combined effects of g-tensor and intramolecular dipolar interactions. Nonsecular contributions to the linewidth have also been included. Quadrupole terms[34] and cubic terms resulting from first order corrections to the wave function[35] have been estimated to be negligible. If an isotropic τ_R is assumed, it is possible to obtain independent estimates from both B and C, the coefficients of the $\tilde{M}$ and $\tilde{M}^2$ terms respectively. It is found from results of such calculations, for a representative group of temperatures in both systems, that the two estimates differ systematically by an amount which is significantly greater than the experimental error. That is, for frozen H_2O and glycerol-H_2O the ratio of τ_R calculated from C to that from B is 1.3±0.1 and 1.5±0.1, respectively.

It can be seen from the expressions given by Kooser *et al.*,[8] that when $\omega_0^2\tau_R^2 \gg 1$ and $\omega_{n\pm}^2\tau_R^2 \ll 1$ an isotropic rotational diffusion model predicts that

$$B/C = (16/5)J^{(DG_2)}(0)B_0/J^{(D)}(0), \qquad (4)$$

which is independent of τ_R. In Figs. 7 and 8, a comparison is made between the experimentally observed values of B vs C and those calculated assuming isotropic rotational diffusion. It is evident that the experimental results cannot be explained in this manner.

Two alternate possibilities are known to exist.[13,23] They are (1) the possibility of anisotropic rotational diffusion, and (2) isotropic modulation of hyperfine and g-tensor terms. Our analysis, given below, is in terms of (1). We believe the strongest argument against (2) is the simple fact that the ratio of C/B remains virtually constant over the whole motionally narrowed region where B and C themselves vary by two orders of magnitude and is virtually the same in frozen water

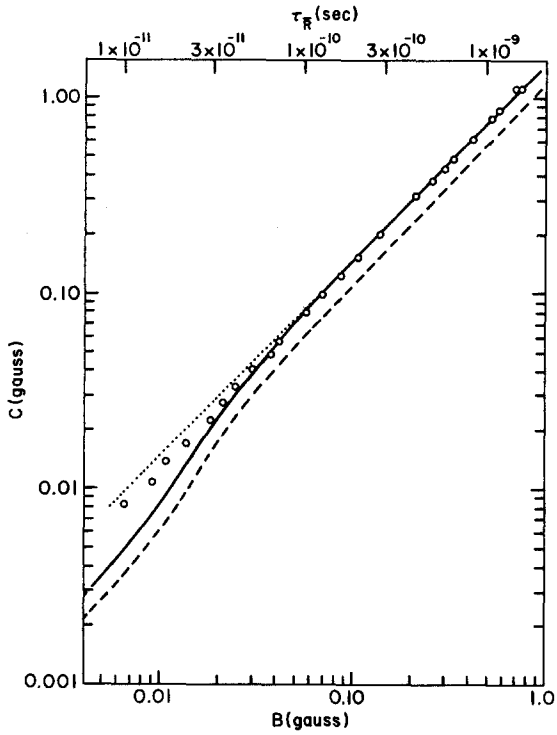

FIG. 7. A comparison of experimental and calculated values of B versus C for PADS in frozen H_2O. — and - - - are calculated from Eq. (5) for $N=2.9$ and 1.0 respectively. ··· is for $N=2.9$ neglecting nonsecular terms in Eq. (5). Experimental points are designated by (0.) Note that both B and C are plotted on log scales. Thus the absolute difference between the experimental and calculated curves is less than 5 mG for $N=2.9$ and as large as 200 mG for $N=1$.

and in glycerine–water. This appears to be a very strong argument against any modulation process supplementary to the rotational diffusion, as there is little reason to suppose the supplementary process would have the same T (or more precisely η/T) dependence as the rotational motion. However, for anisotropic rotation, wherein the rotational-diffusion tensor itself has a single specific temperature dependence, the constancy of B/C must follow. It is shown in the discussion below that the experimental results in the motional-narrowing region can readily be fitted with an axially-symmetric rotational diffusion model. It is also shown in our discussion of the slow-motional region that adequate simulation of these spectra requires the assumption of anisotropic rotational reorientation, and for the slow-motional region the effects of (1) and (2) would be qualitatively different (see below).

X-ray crystallography studies of the dimer $K_4(PADS)_2$, indicate that $r_y \approx 2.9$ Å, $r_x \approx 2.2$ Å, and $r_z \approx 1.8$ Å for PADS, where r_i are the approximate molecular radii.[36] This also suggests the possibility of anisotropic rotational diffusion,[13] although the effects of the ionic charge on the motion are not immediately evident.

In order to simplify the analysis, it is assumed that the rotational-diffusion tensor is axially symmetric.[37] We define the principal axes of the diffusion tensor as x', y', and z' with z' the symmetry axis. Then, R_3 is the rotational-diffusion component about z' while R_1 gives the components about x' and y'. The X-ray data suggests that the z' axis should correspond to the molecular y axis, but we do not wish to make such an assignment *ad hoc*. However, the C_{2v} symmetry expected for the radical, when the SO_3^- groups are averaged over their internal motions, suggests that the x, y, z axis system is equivalent (within a displacement of origins) to the x', y', z' axis system, except for the labelling of axes. The following expression is obtained:

$$T_2^{-1}=M^2(4\pi^2/5)\xi^2((D^{(0)})^2\tau(0)\{(8/3)-[1+\omega_a^2\tau(0)^2]^{-1}-\tfrac{1}{3}[1+\omega_0^2\tau(0)^2]^{-1}\}+2(D^{(2)})^2\tau(0)\times\{(8/3)-[1+\omega_a^2\tau(2)^2]^{-1}-\tfrac{1}{3}[1+\omega_0^2\tau(2)^2]^{-1}\})+M(\pi/10)\omega_0\xi(g^{(0)}D^{(0)}\tau(0)\{(16/3)+4[1+\omega_0^2\tau(0)^2]^{-1}\}+2g^{(2)}D^{(2)}\tau(2)\times\{(16/3)+4[1+\omega_0^2\tau(2)^2]^{-1}\})+I(I+1)(4\pi^2/5)\xi^2((D^{(0)})^2\tau(0)\{[1+\omega_a^2\tau(0)^2]^{-1}+(7/3)[1+\omega_0^2\tau(0)^2]^{-1}\}+2(D^{(2)})^2\tau(2)\{[1+\omega_a^2\tau(2)^2]^{-1}+(7/3)[1+\omega_0^2\tau(2)^2]^{-1}\})+(\omega_0^2/80)((g^{(0)})^2\tau(0)\times\{(8/3)+2[1+\omega_0^2\tau(0)^2]^{-1}\}+2(g^{(2)})^2\tau(2)\times\{(8/3)+2[1+\omega_0^2\tau(2)^2]^{-1}\})+X, \quad (5)$$

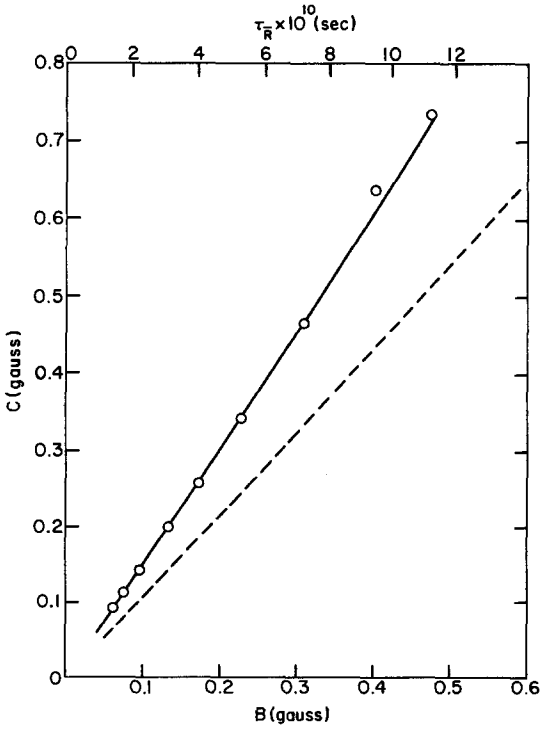

FIG. 8. A comparison of experimental and calculated values of B versus C for PADS in 85% glycerol–H_2O. — and - - - are calculated from Eq. (5) for $N=4.7$ and 1.0 respectively. Experimental points are designated by (0).

where $\xi=(1/2\pi)\mid\gamma_e\mid\gamma_n\hbar$, $\omega_{n\pm}=\pm\omega_n+\frac{1}{2}a_N\mid\gamma_e\mid\approx\frac{1}{2}a_N\mid\gamma_e\mid=\omega_a$ and X is the residual width; also,

$$\tau_{L,m}^{-1}=R_1L(L+1)+(R_3-R_1)m^2, \qquad (6)$$

where $\tau_{2,0}^{-1}=\tau(0)^{-1}=6R_1$ and $\tau_{2,\pm2}^{-1}=\tau(2)^{-1}=2R_1+4R_3$. The irreducible tensor components of **A** and **g**, $D^{(m)}$ and $g^{(m)}$ in Eq. (5), must be expressed in the molecular coordinate system x', y', and z' of the rotational-diffusion tensor. Further details are given elsewhere.[2,13,18] The $\omega_{n\pm}$ dependence of the pseudo-secular terms is included explicitly in Eq. (5). However, $(1+\omega_{n\pm}{}^2\tau_{L,m}{}^2)^{-1}\approx1$ except in the limit where the condition that $\mid\mathcal{H}_1(t)\mid\tau_R\ll1$ is no longer fulfilled.

It is useful, in order to discuss the axially symmetric rotational diffusion, to introduce two new diffusion parameters: $N=R_3/R_1$ and $\bar{R}=(R_3R_1)^{1/2}$. We note that for $\omega_0{}^2\tau_{2,m}{}^2\gg1$, and $\omega_a{}^2\tau_{2,m}{}^2\ll1$, B/C is independent of $\bar{R}$, but is a function of N (including the particular assignment of the x, y, or z axis as the z' axis). A careful analysis of the experimental linewidth results over the whole motional narrowing region, which is summarized, in part, in Table II, shows that $z'=y$ is the *only* choice that can explain our results. For this choice we obtain $N\simeq2.9\pm1$ and 4.7 ± 1 for PADS in frozen H_2O and glycerol-H_2O, respectively. The error limits include the experimental deviation in B/C and small uncertainties in the molecular parameters. Thus, our results imply faster rotation about the molecular y axis. The experimental results and predicted curves of B vs C for these choices of N are given in Figs. 7 and 8 for frozen H_2O and glycerol-H_2O solvents, respectively. The predicted curves for $N=1$ (isotropic tumbling) are also shown, and one clearly sees their disagreement with the experiment results, as we have already pointed out.

It is seen in Fig. 7 [for the region where nonsecular terms are negligible $(\omega_0{}^2\tau_{2,m}{}^2\gg1)$] and in Fig. 8 that a single unique choice of the value of N fits the experimental data very well. The agreement is not as good in Fig. 7 for the region where nonsecular terms become important. However, if we choose to neglect these nonsecular terms, the predicted curve (dotted line in Fig. 7) gives somewhat better agreement with experiment. The experimental results actually lie between the two predicted curves. It is as though nonsecular terms are not properly represented, in this case, by the usual spin-relaxation theory expressions.[2,3] We note first that the nonsecular terms are proportional to the function $\tau_{2,m}/(1+\omega_0{}^2\tau_{2,m}{}^2)$, which is a maximum at $\tau_{2,m}=\omega_0{}^{-1}=1.75\times10^{-11}$ sec. Our shortest values of $\tau_{2,m}$ obtained near the melting point are about 1×10^{-11} sec. Thus, our results are in the region where $\omega_0{}^2\tau_{2,m}{}^2$ is still not negligible. We note that in careful studies of PADS in water at room temperature the ratio $C/B=0.53\pm0.23$ is obtained with an isotropic $\tau_{2,m}\simeq3\times10^{-12}$ sec. (The experimental error in the very small values of B and C compared to A is too great to distinguish between isotropic and anisotropic motional models from these results.) One finds from Eq. (5), that only when nonsecular terms become important can C/B become significantly less than unity (barring enormous changes in N). Thus, for the extreme narrowing region $(\omega_0{}^2\tau_{2,m}{}^2\ll1)$ there is very clear evidence for the contribution of the nonsecular terms to the width. It is only in the intermediate region of $\omega_0\tau_{2,m}\sim1$ that there might be some anomaly. This is further discussed below.

Values of $\bar{R}$ and N were obtained for each temperature by fitting the experimental results for B and C

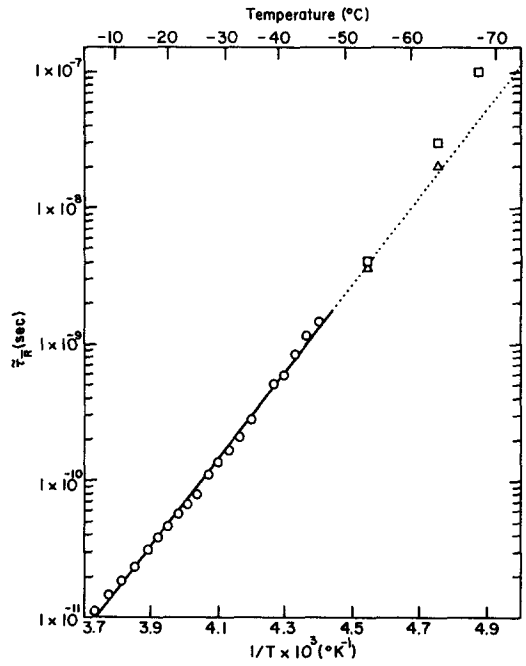

FIG. 9. $\tilde{\tau}_{\bar{R}}$ versus $1/T$ for PADS in frozen H_2O. Motional-narrowing results are designated by (○). Values of $\tilde{\tau}_{\bar{R}}$ obtained from slow-motional simulations are designated by (△) for free diffusion and (□) for Brownian diffusion models. The solid line represents a least square fit to the motional-narrowing results.

TABLE II. Calculated C/B as a function of N.[a]

N	C/B $z'=z$[b]	($=1.45\pm0.05$ from experiment) $z'=y$[b]	$z'=x$[b]
6	1.10	1.93	0.79
3	1.11	1.48	0.92
1	1.13	1.13	1.13
$\frac{1}{3}$	1.15	1.00	1.26
$\frac{1}{6}$	1.17	0.97	1.30[c]

[a] These values are calculated from Eq. (5) for the g and A values given in Table I for PADS in frozen D_2O. It is assumed that $\omega_0{}^2\tau_{L,m}{}^2\gg1$ and $\omega_{n\pm}{}^2\tau_{L,m}{}^2\ll1$.

[b] z' is the symmetry axis of the diffusion tensor and x, y, and z are the molecular fixed axes (see text).

[c] $\lim_{N\to0}(C/B)=1.35$.

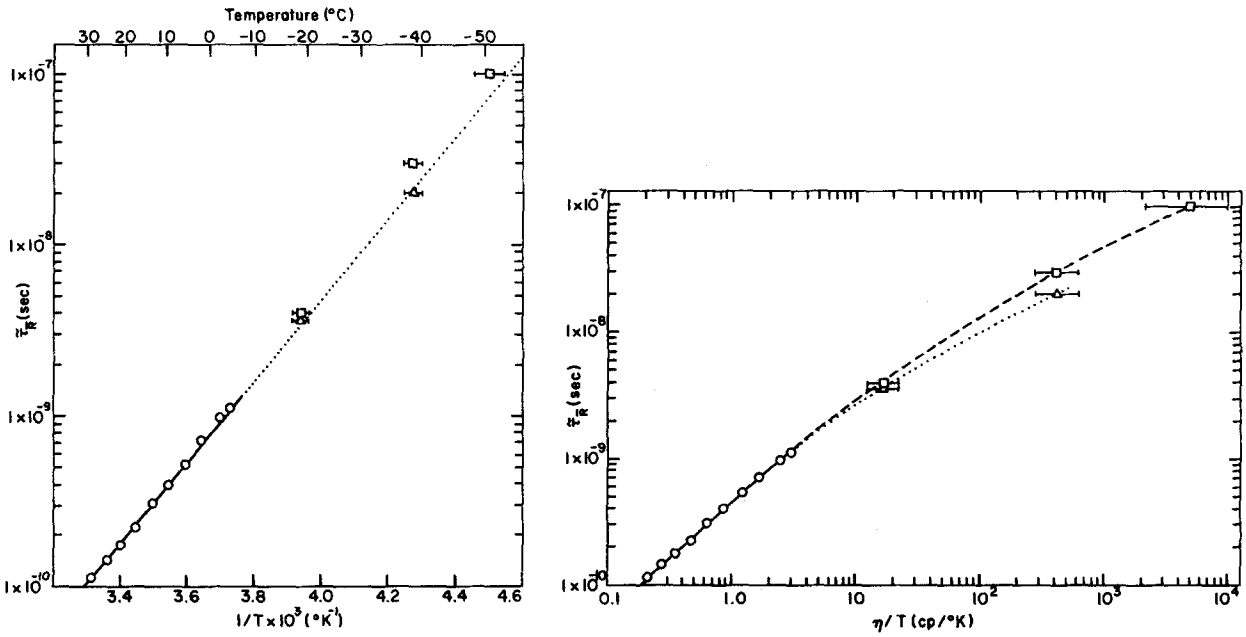

FIG. 10. $\tilde{\tau}_{\bar{R}}$ versus $1/T$ and η/T for PADS in 85% glycerol-H_2O. Motional-narrowing results are designated by (○). Values of $\tilde{\tau}_{\bar{R}}$ obtained from slow-motional simulations are designated by (△) for free diffusion and (□) for Brownian diffusion models. (a) Variation with $1/T$. Solid line is a least squares fit to the motional-narrowing results. (b) Variation with η/T.

to Eq. (5). The mean $\tau_{\bar{R}} \equiv (6\bar{R})^{-1}$ is shown for the different temperatures on the x-axis scale in Figs. 7 and 8 and $\tau_{\bar{R}}$ is given explicitly in Figs. 9 and 10 as functions of $1/T$ for frozen H_2O and both $1/T$ and η/T for glycerol-water solvent, respectively. The value of N remained constant at 4.7 ± 0.3 for glycerol-H_2O and 2.9 ± 0.3 for ice, over the range for which $\omega_0^2\tau_{2,m}^2 \gg 1$, where the error limits reflect the experimental deviation in B/C. No attempt was made to correct Eq. (5) for the peculiar results just discussed in the region $\omega_0\tau_{2,m} \sim 1$ and this leads to an increase in the value of $\bar{N}$ estimated from Eq. (5). (The values of $\tau_{\bar{R}}$ one would obtain from neglecting nonsecular terms in Eq. 5, hence keeping $N \approx 3$, would not differ by more than 5% from those given.)

It is possible to estimate a theoretical value for A from Eq. (5) as well as the expected contribution from spin–rotational interaction by utilizing the experimental values of $\bar{R}$ and N.

The simplest expression for the spin–rotational linewidth contribution for isotropic Brownian reorientation is [38,39]

$$(T_2^{-1})^{SR} = \sum_i (g_i - g_e)^2/9\tau_{\bar{R}}, \qquad (7)$$

where g_e is the free electron g value.

The linewidth contributions to A estimated from Eqs. (5) and (7) are shown in Figs. 11 and 12 and are compared with the experimental results. These estimated contributions cannot completely account for the observed linewidth.[40] The residual X varies from about 0.1 G for the shorter values of $\tau_{\bar{R}}$ to about 0.2 G (for water solvent) and 0.3 G (for glycerol–water) for slower $\tau_{\bar{R}}$. Thus, it is not very temperature dependent compared to A itself. The observation of a "temperature-independent" contribution to the PADS line-

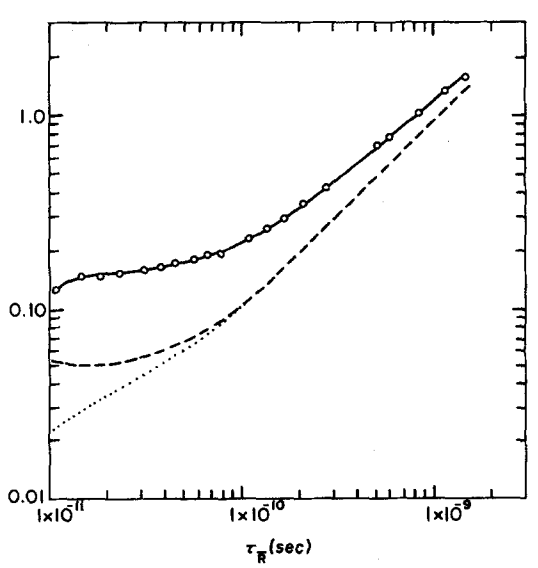

FIG. 11. A versus $\tau_{\bar{R}}$ for PADS in frozen H_2O. Experimental values are designated by (○). - - - is calculated from Eqs. (5) and (7) and includes dipolar, g tensor, and spin–rotational contributions; ··· neglects spin–rotation.

width in aqueous solution of magnitude 0.097±0.010 G has already been reported.[8]

B. Slow-Motional Simulations

The basic theory for simulating slow-motional ESR lineshapes has been developed in I. Simulated spectra for a $S=\frac{1}{2}$, $I=1$ "nitroxide" are shown, but the **g** and **A** tensor were taken as axially symmetric and isotropic Brownian rotational diffusion was assumed. The spectra that are simulated under these simplified conditions are qualitatively similar to the experimental spectra we have obtained.

The method is readily extended to include asymmetric **g** and **A** tensors as well as asymmetric Brownian rotational diffusion, although for reasons of simplicity we consider only axially symmetric diffusion. The procedure involves the expansion of the lineshape in terms of a complete orthogonal set of eigenfunctions of the Markovian rotational diffusion operator. The Wigner rotation matrices $\mathfrak{D}_{KM}{}^{L}(\Omega)$ with eigenvalues $E_{K,M}{}^{L}=\tau_{L,K}{}^{-1}$ as given by Eq. (6) provide such a set for axially symmetric Brownian rotational diffusion. Convergent solutions may be obtained by terminating the expansion at a sufficiently large value of $L=n$. In general, the larger the value of $|\,\mathcal{K}_1(t)\,|\,\tau_{\bar{R}}$, the larger the value of n must be. Discussion of convergence given in I (and below) is again appropriate here. We note that for $|\,\mathcal{K}_1(t)\tau_R\,|\ll 1$, convergence can be obtained with $n=2$, and this yields essentially the same results as the earlier relaxation theories. The detailed equations that are used are given in the Appendix.

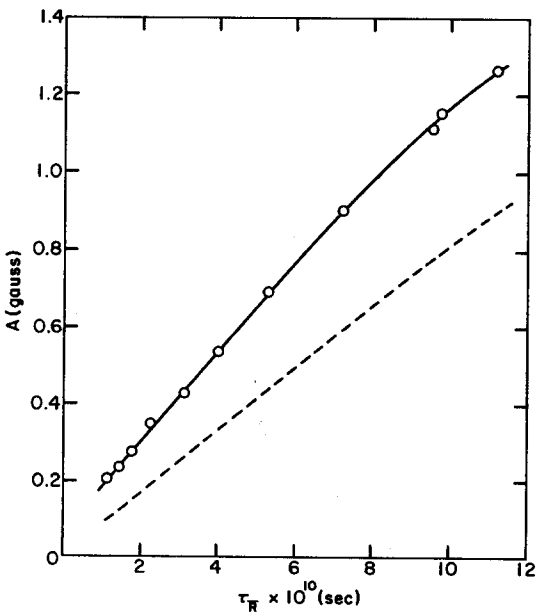

FIG. 12. A versus $\tau_{\bar{R}}$ for PADS is 85% glycerol–H_2O. Experimental points are designated by (O). - - - is calculated from Eq. (5) and includes dipolar and g-tensor contributions. (Spin–rotational contributions are calculated as being negligible.)

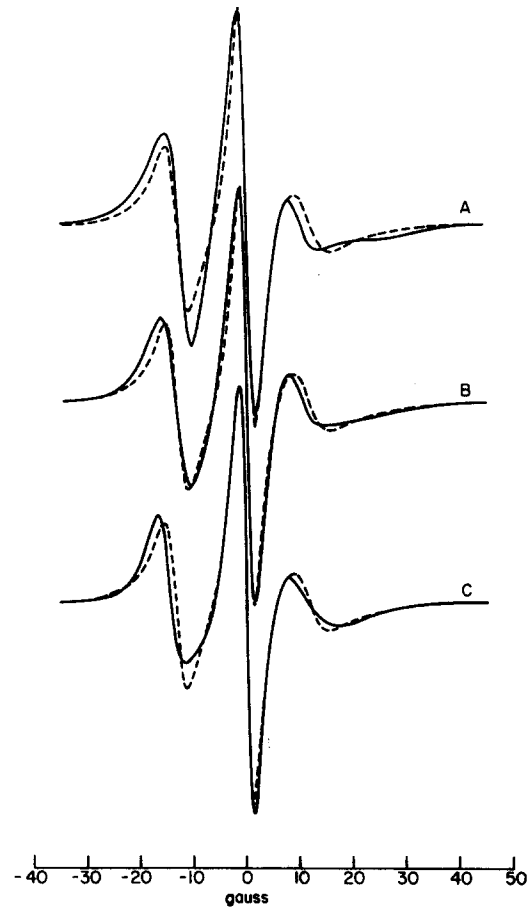

FIG. 13. A comparison of simulated and experimental spectra for PADS in frozen D_2O at $T=-50$°C. - - - is the experimental spectrum. — is calculated for Brownian diffusion with $\tilde{\tau}_{\bar{R}}=2$, $X=0.2$ G, and A $N=1$, B $N=3$, and C $N=6$.

The rotational diffusion correlation time $\tau_{\bar{R}}$ is expressed as a dimensionless parameter:

$$\tilde{\tau}_{\bar{R}}=6\,|\,F(0)\,|\,\tau_{\bar{R}}, \tag{8a}$$

where

$$F(0)=(2/3)^{1/2}\hbar^{-1}\beta_e B_0 g^{(0)}. \tag{8b}$$

For Brownian rotational diffusion, this is equivalent to $|\,F(0)\,|/\bar{R}$ used in I.

For PADS in frozen D_2O, the residual linewidth X varies from about 0.2 G in the motional-narrowing region to about 1.1–1.5 G in the rigid limit. Thus X increases with increasing τ_R, and in the slow-motional region its value must lie between these two extremes. The values of X utilized in the simulated spectra are adjusted to give optimum agreement with the observed spectra.

Experimental spectra for PADS in frozen D_2O obtained at three different temperatures: −50°, −60°, −65°C, which are representative of the slow-motional region, were chosen for purposes of spectral simulation. The experimental and simulated spectra are shown in Figs. 13, 14, and 15, respectively. In each figure, the

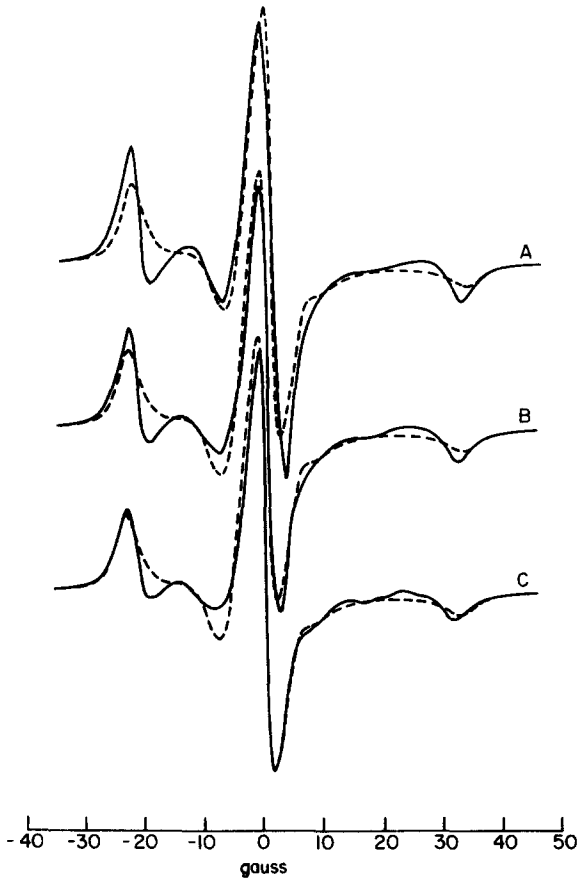

FIG. 14. A comparison of simulated and experimental spectra for PADS in frozen D_2O at $T=-60°C$. - - - is the experimental spectrum. — is calculated for Brownian diffusion with $\tau_{\bar{R}}=15$, $X=0.6$ G, and A $N=1$, B $N=3$, and C $N=6$.

experimental spectrum is superposed (in dashed lines) on a simulated spectrum obtained for one of the values of $N=1$, 3, or 6. The experimental spectrum in Fig. 13, for $-50°C$, is characteristic of rotational motion that is sufficiently rapid to yield a three line "motionally-narrowed type" spectrum but too slow for the usual relaxation theories to apply; in Fig. 15, for $-65°C$, the rotational motion has slowed sufficiently so that the observed spectrum has many of the features of the rigid limit spectrum, cf. Fig. 6; Fig. 14, for $-60°C$, is intermediate between these two extremes.

For the $-50°C$ spectrum in Fig. 13, the best overall agreement is obtained with simulations for which $\tilde{\tau}_{\bar{R}}\approx 2$. The initial comparison is made with respect to the width of the $\tilde{M}=0$ line and the relative amplitudes of the $\tilde{M}=+1$ and $\tilde{M}=0$ lines, since these characteristics are almost independent of N in accordance with our observations for the motionally narrowed region. Figure 13, curves A–C correspond to values of $N=1$, 3, and 6, respectively. The primary effect of varying the value of N is to change the relative amplitude of the $\tilde{M}=-1$ line, but there are other shape changes. It is clear from the comparisons in Fig. 13, that it is necessary to assume anisotropic diffusion to obtain even moderate agreement between experimental and simulated spectra. The best overall fit is obtained for $N\approx 3$ and $X=0.2$ G. Thus, it appears that the rotational motion can still be expressed in terms of the motional-narrowing parameters, as one would naturally expect.

It is useful, for purposes of discussing slow-motional spectra such as those in Figs. 14 and 15, to define an ordering parameter $S=A_z'/A_z$, similar to the one used by Hubbell and McConnell,[1a] where A_z' is one-half the distance between the outer hyperfine extrema, as measured in the slow-motional spectra, and A_z is the rigid-limit value for the same quantity. Thus $S\leq 1$. Experimentally it is found that S increases with decreasing temperature. It is observed, from the spectral simulations, that S increases monotonically with $\tilde{\tau}_{\bar{R}}$ and for a specific rotational model, (see below) its value is almost invariant to changes in N and to small changes in the **g** and **A** tensors, (e.g., the value of S calculated for $\tilde{\tau}_{\bar{R}}=15$ for axially symmetric parameters[4] is the same as that calculated for the asymmetric parameters used in Fig. 14). Thus it seems reasonable that a useful criterion for agreement between experimental and simulated spectra is that their respective values for this parameter be the same (within the experimental error in A_z). This criterion was used for initial comparisons for the spectra in Figs. 14 and 15.

The best overall agreement for the $-60°C$ spectrum in Fig. 14 is obtained for $\tilde{\tau}_{\bar{R}}\simeq 15$ and $X\approx 0.6$ G, and again comparisons for $N=1$, 3, and 6 are shown. The

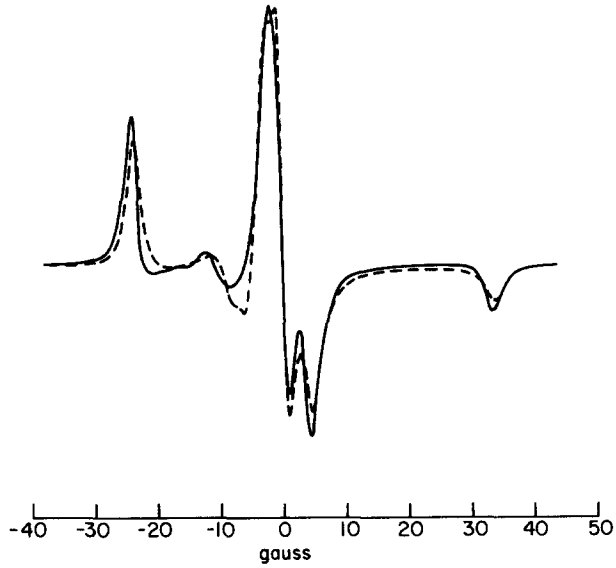

FIG. 15. A comparison of simulated and experimental spectra for PADS in frozen D_2O at $T=-65°C$. - - - is the experimental spectrum. — is calculated for Brownian diffusion with $\tilde{\tau}_{\bar{R}}=50$, $X=0.9$ G, and $N=3$.

spectra for $N=3$ and 6 show a decrease in the amplitude of the outer hyperfine extrema relative to the central region, a narrowing of the peak to peak width of the broad center line and an increase in its anisotropy, all of which contribute to an overall improvement in the fit. However, the agreement between experimental and simulated spectra is not entirely satisfactory with significant discrepancies in the regions -10--20 G and $+15$--$+25$ G. It is in fact difficult to determine whether $N=3$ or 6 gives a more satisfactory agreement.

The best agreement for the experimental spectra observed at -65°C (in Fig. 15) is obtained for $\tilde{\tau}_{\bar{R}}\approx 50$ and $X\approx 0.9$ G. The calculated spectrum for $N=3$ is shown in Fig. 15. The agreement in the field range -10 to -20 G and $+15$ to $+25$ G has improved substantially, and the overall fit is good except for the presence of a shoulder on the experimental spectrum that does not appear on the simulated spectrum. This particular lack of agreement can be partially attributed to the fact that: (1) at higher $\tilde{\tau}_{\bar{R}}$ values, ($\tilde{\tau}_{\bar{R}}>30$) the spectra are more sensitive to slight inaccuracies in the **A** and **g** tensors. Many of the differences between the experimental and simulated spectra for $\tilde{\tau}_{\bar{R}}=50$ can be noted in a comparison of the comparable rigid spectra, and it would be unreasonable to expect better agreement. (2) The orientational dependence of the residual linewidth, that was observed for the rigid-limit spectrum, was not included in the slow-motional simulations.[41] This orientational dependence could be important at $\tilde{\tau}_{\bar{R}}=50$ where a residual linewidth near the rigid limit was observed. (3) Experimentally it is observed that $\tilde{R}$ is very sensitive to temperature for $\tilde{\tau}_{\bar{R}}\gtrsim 15$. The temperature difference between $\tilde{\tau}_{\bar{R}}$ of 50 and 15 is only about 5°C. Thus a single experimental spectrum consists of a significant range of $\tilde{\tau}_{\bar{R}}$ values due to the temperature variation (± 0.5°C) over the large sample. It is our belief, however, that the above reasons can not account for the lack of agreement between the experimental spectrum in Fig. 14 (-60°C) and the best spectra simulated with a Brownian rotational diffusion model. Thus, it was thought worthwhile to consider other rotational models.

C. Models for Rotational Reorientation

A number of different models for rotational reorientation can be proposed. We have found that a recent discussion by Egelstaff[42] of rotational models is particularly useful for our method of simulation of ESR spectra in the slow tumbling region. Egelstaff considers three possible cases of molecular reorientation: (a) Brownian rotational diffusion; (b) jump diffusion, in which the molecule has a fixed orientation for time τ and then "jumps" instantaneously to a new orientation; and (c) free diffusion for which the molecule reorients freely for the time τ (i.e., inertial motion) and then jumps instantaneously to a new orientation. When the motion is spherically symmetric, one can summarize the results for these models as:

$$\text{(a)}\quad \tau_L^{-1}=L(L+1)R, \tag{9}$$

$$\text{(b)}\quad \tau_L^{-1}=\tau^{-1}\left[1-(2L+1)^{-1}\int_0^{\pi} d\epsilon W(\epsilon)\times\left(\frac{\sin(L+\frac{1}{2})\epsilon}{\sin\frac{1}{2}\epsilon}\right)\right], \tag{10}$$

where $W(\epsilon)$ is the distribution function for diffusive steps by angle ϵ and is normalized so that

$$\int_0^{\pi} W(\epsilon)\,d\epsilon=1,$$[43]

and

$$\text{(c)}\quad \tau_L^{-1}\sim L(L+1)R/[1+L(L+1)R\tau]^{1/2}. \tag{11}$$

We note that the value of $\tau_{L,M}$ for (b) depends upon an appropriate choice of $W(\epsilon)$. Egelstaff suggests as a convenient form:

$$\text{(i)}\quad W(\epsilon)=A\sin(\tfrac{1}{2}\epsilon)\exp(-\epsilon/\theta), \tag{12a}$$

where A is a normalization constant. If, $\theta<\pi$, one obtains

$$\tau_L^{-1}=L(L+1)R/[1+R\tau L(L+1)] \tag{12b}$$

and

$$\langle\epsilon^2\rangle_{Av}=6\theta^2, \tag{12c}$$

when the diffusion coefficient is defined in the usual way as:

$$R=\langle\epsilon^2\rangle_{Av}/6\tau. \tag{13}$$

We summarize other, possible choices:

(ii) Exponential distribution

$$W(\epsilon)=A\exp(-\epsilon/\theta),\qquad \theta<\pi, \tag{14a}$$

$$\tau_L^{-1}=\left(\frac{6R}{(2L+1)}\right)\sum_{P=1}^{L}\frac{P^2}{(1+9\tau^2R^2P^2)}, \tag{14b}$$

and

$$\langle\epsilon^2\rangle_{Av}=2\theta^2. \tag{14c}$$

(iii) Gaussian distribution

$$W(\epsilon)=A\exp(-\epsilon^2/\theta^2),\qquad \theta<\pi, \tag{15a}$$

$$\tau_L^{-1}=\left[\frac{12R}{(2L+1)\theta^2}\right]\left[L-\sum_{p=1}^{L}\exp(-\tfrac{1}{2}\theta^2p^2)\right], \tag{15b}$$

and

$$\langle\epsilon^2\rangle_{Av}=\theta^2. \tag{15c}$$

(iv) Random distribution

$$W(\epsilon)=1/\pi, \tag{16a}$$

$$\tau_L^{-1}=(18R/\pi^2)[2L/(2L+1)], \tag{16b}$$

and

$$\langle\epsilon^2\rangle_{Av}=\pi^2/3. \tag{16c}$$

With the exception of (iv), it is easy to show that, as

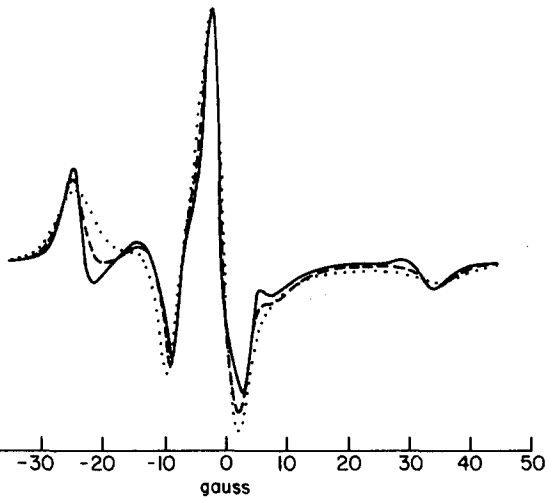

FIG. 16. A comparison of line shapes simulated for Brownian, free, and jump diffusion models. —: Brownian diffusion $\tilde{\tau}_R=15$, - - -; free diffusion $\tilde{\tau}_R=10$, and •••: jump diffusion $\tilde{\tau}_R=7$. The spectra are calculated for an "axial" nitroxide with the parameters given in I.

θ becomes infinitesimally small, all these models are equivalent to Brownian rotational diffusion, yielding Eq. (9). On the other hand, for large values of θ, all these models are approximated by $\tau_{L,M}\sim\tau$ for $L>0$.

The Eq. (11) is a very crude approximate form for free diffusion. More accurately one has, for the correlation of the Wigner rotation matrices[44,45]:

$$\langle \mathfrak{D}_{KM}{}^{L*}(t)\mathfrak{D}_{KM}{}^{L}(0)\rangle = \exp\{L(L+1)R\tau[1-t/\tau-\exp(-t/\tau)]\} \quad (17)$$

as opposed to simple exponential decay of form $\exp(-t/\tau_L)$ obtained from models (a) and (b). Because free diffusion [model (c)] includes inertial effects, the orientation of the molecule is not properly described as a simple Markovian process, but is rather the projection of a higher dimensional Markovian process including the angular momentum as well as the orientation.[44,45] However for times $t\gg\tau$, Eq. (17) again predicts Brownian diffusive behavior, Eq. (9). The approximation, Eq. (11), is obtained from the best Lorentzian fit to the Fourier transform of a modified form of Eq. (17).[42] We use Eq. (11) in a straightforward manner rather than rederive the whole formulation given in the Appendix for the more complex Markovian process.

The primary point to be made is that the L dependence of $\tau_{L,M}$ is a sensitive function of the nature of the reorientational model. Since the ESR spectra in the slow tumbling region are simulated in terms of an expansion in $\mathfrak{D}_{KM}{}^{L}$, it is natural to expect that significant lineshape changes can result from utilizing different models. However, this is expected only for intermediate values of $\tilde{\tau}_{\bar{R}}$, since, when $\tilde{\tau}_{\bar{R}}$ becomes very large, the rigid limit spectrum is obtained for all models. When $\tilde{\tau}_{\bar{R}}$ is short enough, simple Lorentzian ESR lineshapes are obtained from all the models.

In order to demonstrate how these models affect the ESR spectrum, the axially symmetric nitroxide program was utilized with values of $\tau_{L,M}$ given by

$$\tau_L{}^{-1}=B_L L(L+1)R \quad (18)$$

with the "model parameter" $B_L=1$ for Brownian motion; $B_L=[1+L(L+1)]^{-1}$ for jump diffusion, model (i) and $R\tau=1$; $B_L=[1+L(L+1)]^{-1/2}$ for free diffusion and $R\tau=1$. Hereafter, for simplicity, we usually refer to these choices of B_L as Brownian, jump, and free diffusion, respectively. For purposes of comparison we generalize our definition of $\tau_{\bar{R}}$ to:

$$\tau_{\bar{R}}(B)=(6B_2\bar{R})^{-1} \quad (19)$$

with $\tilde{\tau}_{\bar{R}}$ again given by Eq. (8a). Thus, in the motionally narrowed region, where only the $L=2$ term is important, it follows from Eq. (18) that all models yield the same Lorentzian width for the same value of $\tilde{\tau}_{\bar{R}}$.

A superposition of nitroxide line shapes for the three choices of B_L is shown in Fig. 16. The value of $\tilde{\tau}_{\bar{R}}$ for Brownian diffusion is the intermediate value of 15. It was found that for jump and free diffusion, it was necessary to use smaller values of $\tilde{\tau}_{\bar{R}}$: 7 and 10, respectively, in order that the value of S be nearly the same in all cases. It is quite clear from this figure that there are significant differences in the line shapes. As one proceeds from Brownian, to free, to jump diffusion, one obvious feature is the effective broadening of the lines. As we have noted, significant discrepancies between the experimental spectrum and anisotropic Brownian simulation were found in the regions -10 to -20 G and 15 to 25 G (referred to as the critical regions). These discrepancies, i.e., curvature, tend to smooth out in progressing to free and jump diffusion simulations. It is our belief that the free diffusion simulation gives the best qualitative comparison with the experimental spectrum.[45a] It has reduced the discrepancies characteristic of the Brownian diffusion simulation in the critical regions, yet it does not have excessively broad outer lines as in the jump diffusion simulation. One can note from Figs. 14 and 16 that for Brownian diffusion the width of the low-field line is rather insensitive to changes in value of N, the anisotropic diffusion parameter, as well as to whether the axial $\mathbf{g}$ and $\mathbf{A}$ parameters[4] are used instead of the true parameters. We shall see this is also true for free diffusion. This suggests that the excessive broadening of the jump diffusion simulation will not be improved by using the true parameters.

The reason for the significant changes in the critical regions with change in model is suggested by Sillescu's discussion of model effects on the simple case of an ESR spectrum of a single absorption line with axially

symmetric g tensor.[7] He found in a comparison of a strong jump model with Brownian diffusion that the simulated spectra are most sensitive to the model in the region where $d\omega(\theta)/d\theta$ is a maximum; $\omega(\theta)$ is the resonance frequency for the orientation θ. An approximate calculation shows that for the rigid axially-symmetric nitroxide spectrum, $d\omega(\theta)/d\theta$ does have maxima in the critical regions.

There is a significant feature in the computer simulation of Fig. 16 that should be pointed out. The convergence of the coupled equations for the coefficients of the $\mathfrak{D}_{KM}{}^{L}$ becomes poorer as one progresses from Brownian, to free, to jump diffusion; this requires values of $n=6$, 10, and 22, respectively, for convergence. The poor convergence of the jump diffusion simulation prevented us from using this model in the general program given in the Appendix. The reason for the good convergence in the case of Brownian diffusion is discussed in I, wherein it is shown that it depends to a large degree on the magnitude of $(\tau_{L+2,K}{}^{-1}-\tau_{L,K}{}^{-1})$ which from Eq. (18) is $4L+6$ for Brownian, and for $L\gg1$ is 2 for free and $4/L^3$ for jump diffusion.

We now consider anisotropic diffusion for the above models. Since there do not appear to be any convenient solutions for anisotropic free or jump diffusion, we have chosen simply to extend our approach of Eq. (18) to the axially symmetric case by rewriting Eq. (6) as:

$$\tau_{L,K}{}^{-1}=B_L[R_1L(L+1)+(R_3-R_1)K^2]. \quad (20)$$

Equation (20) has the virtue that there is only a single adjustable parameter, B_L, in examining effects of different models. It is also very convenient for analyzing the rapid motional linewidths. In effect, we are assuming in Eq. (20) that although the L dependence of $\tau_{L,M}{}^{-1}$ is model dependent, the "quantum-number" K (which is analogous to the projection of the quantum-mechanical rigid rotor angular momentum on the molecular symmetry axis) plays the same relative role in all models.

Spectral simulations for the anisotropic free diffusion model employing the **g** and **A** tensor values given in Table I and Eq. (20) were obtained for comparison with the experimental spectra observed at $T=-50°$ and $-60°$C. (Convergence problems made it difficult to simulate the $-65°$C spectrum.) These simulations are compared with the experimental spectra in Figs. 17 and 18. The choice of $\tilde{\tau}_{\tilde{R}}$ for these two temperatures was based on the criteria previously discussed for the Brownian model and were found to be 1.8 and 10 for $-50°$ and $-60°$C, respectively.

It can be seen in Fig. 17 ($-50°$C), that the qualitative effect of varying N is the same as for Brownian diffusion (cf. Fig. 13). The best fit is obtained for $N=3$, which, except for a slightly too intense $\tilde{M}=-1$ line, is nearly identical to the experimental spectrum. The agreement is clearly better than can be obtained for Brownian diffusion (cf. Fig. 13).

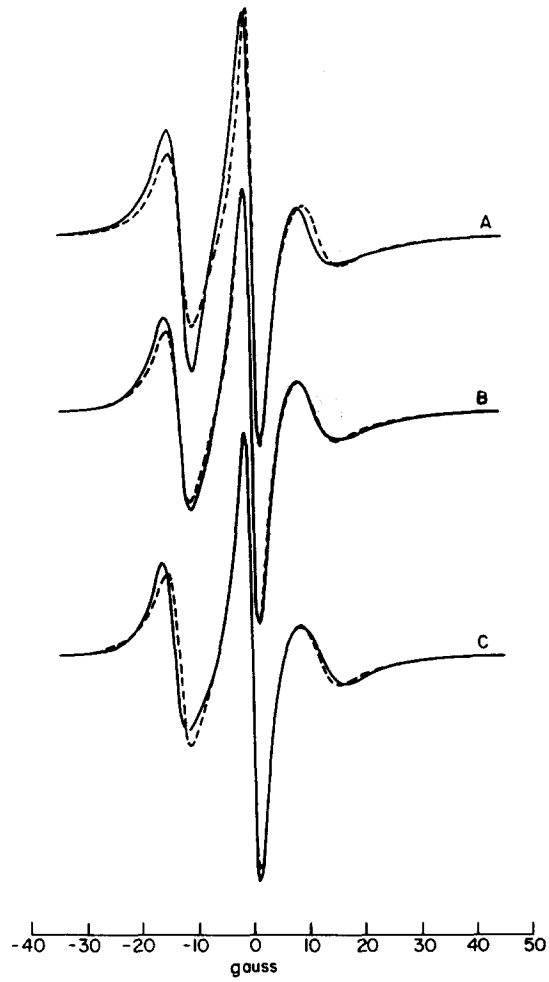

FIG. 17. A comparison of simulated and experimental spectra for PADS in frozen D_2O at $T=-50°$C. - - - is the experimental spectrum. — is calculated for free diffusion with $\tilde{\tau}_{\tilde{R}}=1.8$, $X=0.2$ G, and A $N=1$, B $N=3$, and C $N=6$.

The spectrum simulated for isotropic reorientation at $T=-60°$C is shown in Fig. 18, curve A. It can be seen that the agreement in the region $+15$–$+25$ G has improved substantially, compared to the Brownian models (Fig. 14), and some improvement is noted in the region -10 to -20 G. The agreement between experimental and simulated spectra in this latter region becomes very good for $N=3$ (Fig. 18, curve B). The use of $N=3$ also decreases the amplitude of the outer hyperfine extrema relative to the central region and reduces the peak-to-peak linewidth of the center line yielding better agreement with the experimental spectra.

The simulation for $N=6$ is shown in Fig. 18, curve C. While it shows a little improvement in some details compared to $N=3$, it is on the whole not quite as satisfactory. Thus the best overall fit appears to be for $N\approx3$. The fact that the $N=3$ fit is not better in all respects to that for $N=6$ might possibly be due to

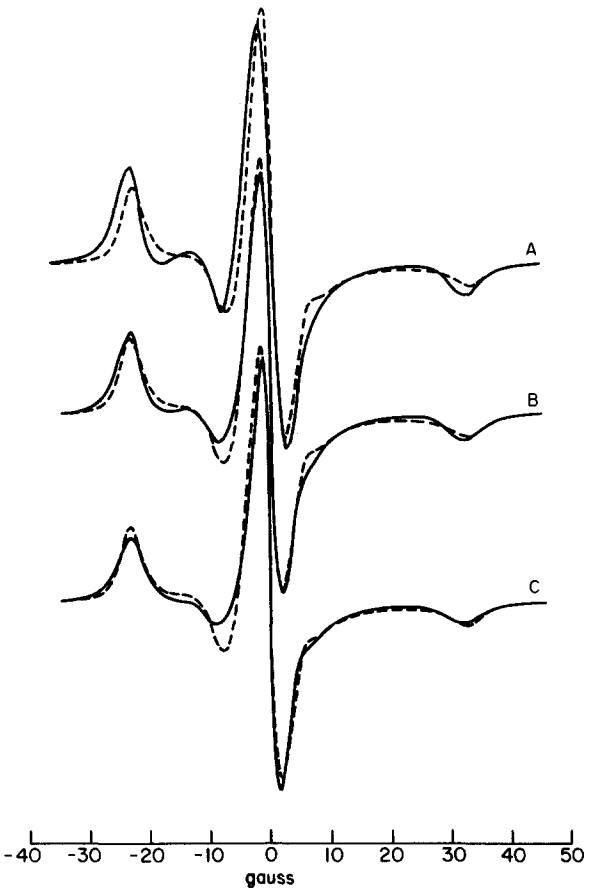

FIG. 18. A comparison of simulated and experimental spectra for PADS in frozen D_2O at $T=-60°C$. - - - is the experimental spectrum. — is calculated for free diffusion with $\tilde{\tau}_{\bar{R}}=10$, $X=0.6$ G, and A $N=1$, B $N=3$, and C $N=6$.

nonaxially symmetric rotational diffusive behavior, which has been neglected in our analysis, and/or to deviations from the simple K dependence assumed in Eq. (20).

We note at this point that the slow tumbling spectra obtained for glycerol–water solvent are almost identical to those in frozen D_2O shown in Figs. 17 and 18. The experimental spectrum shown in Fig. 19, for $T=-39°C$, is very similar to that in Fig. 18. Thus, a similar analysis as that given above for frozen D_2O should apply. However, as soon as the tumbling becomes slow enough ($\tilde{\tau}_{\bar{R}}\gtrsim 15$) the increased residual width X for glycerol–water obscures detailed changes in the line shape. It was still possible to obtain approximate values of $\tilde{\tau}_{\bar{R}}$ by comparing the value of S, which is not very sensitive to N, in the simulated spectra of Figs. 14, 15, and 18 with that observed experimentally.

Given that our particular simple model of free diffusion, where $B_L=[1+L(L+1)]^{-1/2}$, seems to yield simulations that agree well with the observed spectra, it is important to note that the resulting values of the model parameter, B_L, are not entirely unique to this model. Thus for $\tilde{\tau}_{\bar{R}}$ of 1.8 and 10 the simulated spectrum is determined by $L=2$ and 4 and 2, 4, 6, and 8, with marginal contribution from 10 respectively. Over this range of values of L, it is possible to roughly reproduce the values of B_L of the free diffusion case by the jump diffusion models given by Eqs. (12), (14), and (15) and $R\tau\sim 0.2$ with some variation among the models. However, for $L\gtrsim 8$, B_L is significantly lower for the jump models than the free diffusion model used. We may note that all these cases are characterized by $B_2/B_1\simeq 2$. We have not attempted to look for any small spectral differences predicted from these models, nor have we considered other possible models.

We have already noted that all these models will give the same Lorentzian widths for the same values of $\tilde{\tau}_{\bar{R}}$ in the motional narrowing region. This statement is true provided only we use the simple exponential decay of correlations of $\mathfrak{D}_{KM}{}^{L}(t)$ as given, for example, by Eqs. (9)–(11) or (19). In the region where $\tau_{L,K}{}^2\omega_0{}^2\gtrsim 1$, one is now sampling the high-frequency spectrum generated by the rotational reorientation, and from Fourier inversion theorems the short time behavior ($t\sim\omega_0{}^{-1}=1.75\times 10^{-11}$ sec) of this motion becomes important. Thus, for example, in the approximate isotropic free diffusion model Eq. (17) when $t/\tau\ll 1$, (also $t^2<\tau/R$)[45]

$$\langle \mathfrak{D}_{KM}{}^{L*}(t)\,\mathfrak{D}_{KM}{}^{L}(0)\rangle \simeq \exp[-\tfrac{1}{2}L(L+1)Rt^2/\tau] \quad (21)$$

or a Gaussian correlation function, and for $\tau\gtrsim\omega_0{}^{-1}$, the nonsecular spectral densities of Eq. (5) in the motional narrowing region would be determined essentially by the Fourier transform[2] of Eq. (21) or:

$$\tfrac{1}{2}(2\pi\tau\tau_L)^{1/2}\exp(-\tfrac{1}{2}\tau\tau_L\omega_0{}^2) \quad (22)$$

with τ_L defined by Eq. (9), instead of the Debye-type

FIG. 19. ESR spectrum of $5\times 10^{-4}M$ PADS in 85% glycerol–H_2O at $T=-39°C$.

spectral density obtained for $t/\tau \gg 1$ and valid for frequencies $\omega \ll \tau^{-1}$

$$\tau_L/(1+\tau_L^2\omega^2). \quad (23)$$

It thus may be possible, that for PADS in the motional-narrowing region, the nonsecular spectral densities should be approximated by Eq. (22), while the secular and pseudosecular terms are of low enough (near zero) frequency to have spectral densities like Eq. (23). (More general spectral densities for which Eqs. (22) and (23) are the limiting cases are discussed elsewhere.)[46] Suppose then, $R\tau \sim 1$, so $\tau_2 \sim \tau/6$. Then if $\omega_0^2\tau_2^2 = 2$, Eq. (22) is equal to $(7.6\times10^{-3})\tau_2$ while Eq. (23) is $(1/3)\tau_2$. This is just a simple example to show how, if the short-time behavior of the reorientation becomes important, one can hope to explain what appears to be much smaller nonsecular contributions observed experimentally, (cf. Fig. 7) than those calculated from Eq. (5).

Similar general comments apply if the model is jump diffusion. Here, for times $t \ll 1$, the reorientation correlation functions would include motions such as short-term torsional oscillations. One can, in a general way, then replace τ_L in Eq. (23) by a frequency-dependent $\tau_L(\omega)$, such that $\tau_L(\omega) \geq \tau_L(0)$, which includes the short-term effects and yields spectral densities of reduced magnitude.[47] One often approximates such short-term effects as a "relaxing cage."[47] Of course, as the motion slows down, the secular and pseudosecular terms, which are dominant in the slow-motional region, will become more dependent upon the short-time motional behavior, and one would need to consider improved reorientational models for the slow tumbling simulations.

D. Temperature Dependence of Rotational Correlation Times

The dependence of $\tilde{\tau}_{\bar{R}}$ on $1/T$, as shown in the semilog plot of Fig. 9 for frozen water solvent over the whole temperature range studied, yields a good linear fit for the motional-narrowing data. One obtains 14.7 ± 0.2 kcal/mole as the activation energy for the reorientation process. When the slow tumbling results for free or Brownian diffusion are also included, the values are 14.7 ± 0.1 or 15.7 ± 0.2 kcal/mole respectively indicating that the free diffusion results are in better agreement (assuming the validity of a linear fit) with the motional-narrowing results. In the case of glycerol–H_2O [Fig. 10(a)], one obtains respective values of 11.3 ± 0.1, 10.9 ± 0.1, and 11.5 ± 0.1 kcal/mole for motional-narrowing results only, for inclusion of slow tumbling free diffusion points, and for slow tumbling Brownian diffusion points.

It is quite clear, from the fact that PADS rotates so freely in frozen water, that it must be contained in a clathrate cage. Also the existence of clathrate-type cages for PADS in liquid water solution is most likely the reason for its very short correlation time, of the order of 3×10^{-12} sec, as compared to estimated values of 7×10^{-11} sec ($\bar{r}=4$ Å) or 1.3×10^{-11} sec for $\bar{r}=2.3$ Å (neglecting the positions of K^+) as suggested by the x-ray data on $K_4(PADS)_2$.[36] We notice a similar discrepancy in τ_R values for the glycerol–H_2O solvent. Thus at -2.5°C one obtains from Fig. 10 a value for $\tau_{\bar{R}}$ of 9.5×10^{-10} sec, while one estimates, from the Stokes–Einstein relation, 5×10^{-8} sec ($\bar{r}=4$ Å) or 9×10^{-9} sec ($\bar{r}=2.3$ Å). Furthermore, it is seen from Fig. 10(b) that as η/T increases, $\tau_{\bar{R}}$ does not increase at a comparable rate. These results may imply that PADS is in a clathrate-type cage in the glycerol–H_2O solvent. Dielectric relaxation studies on glycerol–H_2O solutions show that τ_D increases more nearly linearly with η/T,[20] unlike our $\tau_{\bar{R}}$ results. However, we do note that for lower values of η/T ($\sim$4.1 cP/°K) the two relaxation times are of the same order ($\tau_{\bar{R}} \sim 1.5\times10^{-9}$ sec and $\tau_D \sim 2.7\times10^{-9}$ sec), but τ_D increases more rapidly with η/T.

The activation energy of 14.7 kcal/mole in ice is very similar to measured activation energies for other rate processes in ice: dielectric, elastic, and proton spin–lattice relaxation as well as diffusion of isotopes. This data is summarized by Onsager and Runnels.[48] However the actual dielectric and elastic relaxation times, which measure molecular reorientation of H_2O molecules presumably due to migration of orientational defects (or Bjerrum faults), are about $5\text{–}6\times10^{-5}$ sec at -10.8°C [48] compared to 1.8×10^{-11} sec for our ESR results on PADS. It should probably be true that for PADS in a clathrate cage, much smaller motions than actual migration of defects, e.g., thermal lattice vibrations, would be sufficient to induce effective reorientations. Onsager and Runnels argue that although activation energies for dielectric relaxation and self-diffusion are similar, differences in absolute magnitude imply there is not a common mechanism for the two processes. A similar comment could apply to our ESR results with so much shorter relaxation times. One wonders, however, whether a deeper analysis of the migration of various proposed kinds of defects etc., in terms of coupling with the cooperative modes of motion in ice (e.g., lattice vibrations), could not still "explain" the remarkable similarity in all these activation energies for rate processes in ice.

V. CONCLUSIONS

It has been shown in this work that the line shape simulations obtained by the stochastic Liouville method, as employed in I, generally agree very well with experimental spectra obtained for PADS in the slow-motional region. It is also demonstrated that the details of the reorientational motion, i.e., anisotropy of the motion, whether it is Brownian, free diffusion, or jump diffusion can reflect itself in the observed experimental

slow tumbling spectra. The analysis given here is consistent with anisotropic motion as well as significant deviations from a Brownian diffusion model. It is anticipated that future work of this type has the potential of probing more deeply into the nature of molecular reorientation processes.

A careful analysis of the motionally narrowed spectra for PADS has also supported the existence of anisotropic reorientation. What appears to be a surprisingly small nonsecular linewidth contribution in the motional narrowing region may also possibly be an indication of deviations of the reorientation from a Brownian model for short times, $\tau \lesssim \omega_0^{-1} = 1.7 \times 10^{-11}$ sec. The surprisingly fast reorientational motion of PADS in both liquid and frozen water and in glycerine is taken to mean that PADS is contained in a clathrate cage in these solvents. We also note that the activation energy for τ_R in ice is very similar to that obtained for other rate processes in ice which, however, have very much longer correlation times.

APPENDIX

The general equations which define the ESR line shape for a nitroxide are given in the form described in detail in I. They are:

$$(2L+1)^{-1}[(\omega-\omega_0+2b)-i(T_2^{-1}+\tau_{L,K}^{-1})]\bar{C}_{K,0}{}^{L}(1)-(F_0+D')\sum_{L'}\begin{pmatrix} L & 2 & L' \\ 0 & 0 & 0 \end{pmatrix}\begin{pmatrix} L & 2 & L' \\ -K & 0 & K \end{pmatrix}\bar{C}_{K,0}{}^{L'}(1)$$
$$-(F_2+D^{(2)\prime})\sum_{L'}\begin{pmatrix} L & 2 & L' \\ 0 & 0 & 0 \end{pmatrix}\left[\begin{pmatrix} L & 2 & L' \\ -K & -2 & (K+2) \end{pmatrix}\bar{C}_{K+2,0}{}^{L'}(1)+\begin{pmatrix} L & 2 & L' \\ -K & 2 & (K-2) \end{pmatrix}\bar{C}_{K-2,0}{}^{L'}(1)\right]$$
$$+\tfrac{1}{2}(D\sqrt{2})\sum_{L'}\begin{pmatrix} L & 2 & L' \\ 0 & -1 & 1 \end{pmatrix}\begin{pmatrix} L & 2 & L' \\ -K & 0 & K \end{pmatrix}\bar{C}_{K,1}{}^{L'}(4,5)+\tfrac{1}{2}(D^{(2)}\sqrt{2})\sum_{L'}\begin{pmatrix} L & 2 & L' \\ 0 & -1 & 1 \end{pmatrix}$$
$$\times\left[\begin{pmatrix} L & 2 & L' \\ -K & -2 & (K+2) \end{pmatrix}\bar{C}_{K+2,1}{}^{L'}(4,5)+\begin{pmatrix} L & 2 & L' \\ -K & 2 & (K-2) \end{pmatrix}\bar{C}_{K-2,1}{}^{L'}(4,5)\right]=\delta_{L,0}\delta_{K,0}, \quad \text{(A1)}$$

$$(2L+1)^{-1}[(\omega-\omega_0)-i(T_2^{-1}+\tau_{L,K}^{-1})]\bar{C}_{K,0}{}^{L}(2)-F_0\sum_{L'}\begin{pmatrix} L & 2 & L' \\ 0 & 0 & 0 \end{pmatrix}\begin{pmatrix} L & 2 & L' \\ -K & 0 & K \end{pmatrix}\bar{C}_{K,0}{}^{L'}(2)$$
$$-F_2\sum_{L'}\begin{pmatrix} L & 2 & L' \\ 0 & 0 & 0 \end{pmatrix}\left[\begin{pmatrix} L & 2 & L' \\ -K & -2 & (K+2) \end{pmatrix}\bar{C}_{K+2,0}{}^{L'}(2)+\begin{pmatrix} L & 2 & L' \\ -K & 2 & (K-2) \end{pmatrix}\bar{C}_{K-2,0}{}^{L'}(2)\right]$$
$$+\tfrac{1}{2}(D\sqrt{2})\sum_{L'}\begin{pmatrix} L & 2 & L' \\ 0 & -1 & 1 \end{pmatrix}\begin{pmatrix} L & 2 & L' \\ -K & 0 & K \end{pmatrix}[\bar{C}_{K,1}{}^{L'}(4,5)+\bar{C}_{K,1}{}^{L'}(6,7)]$$
$$+\tfrac{1}{2}(D^{(2)}\sqrt{2})\sum_{L'}\begin{pmatrix} L & 2 & L' \\ 0 & -1 & 1 \end{pmatrix}\left[\begin{pmatrix} L & 2 & L' \\ -K & -2 & (K+2) \end{pmatrix}[\bar{C}_{K+2,1}{}^{L'}(4,5)\right.$$
$$\left.+\bar{C}_{K+2,1}{}^{L'}(6,7)]+\begin{pmatrix} L & 2 & L' \\ -K & 2 & (K-2) \end{pmatrix}\times[\bar{C}_{K-2,1}{}^{L'}(4,5)+\bar{C}_{K-2,1}{}^{L'}(6,7)]\right]=\delta_{L,0}\delta_{K,0}, \quad \text{(A2)}$$

$$(2L+1)^{-1}[(\omega-\omega_0-2b)-i(T_2^{-1}+\tau_{L,K}^{-1})]\bar{C}_{K,0}{}^{L}(3)-(F_0-D')\sum_{L'}\begin{pmatrix} L & 2 & L' \\ 0 & 0 & 0 \end{pmatrix}\begin{pmatrix} L & 2 & L' \\ -K & 0 & K \end{pmatrix}\bar{C}_{K,0}{}^{L'}(3)$$
$$-(F_2-D^{(2)\prime})\sum_{L'}\begin{pmatrix} L & 2 & L' \\ 0 & 0 & 0 \end{pmatrix}\left[\begin{pmatrix} L & 2 & L' \\ -K & -2 & (K+2) \end{pmatrix}\bar{C}_{K+2,0}{}^{L'}(3)+\begin{pmatrix} L & 2 & L' \\ -K & 2 & (K-2) \end{pmatrix}\bar{C}_{K-2,0}{}^{L'}(3)\right]$$
$$+\tfrac{1}{2}(D\sqrt{2})\sum_{L'}\begin{pmatrix} L & 2 & L' \\ 0 & -1 & 1 \end{pmatrix}\begin{pmatrix} L & 2 & L' \\ -K & 0 & K \end{pmatrix}\bar{C}_{K,1}{}^{L'}(6,7)+\tfrac{1}{2}(D^{(2)}\sqrt{2})\sum_{L'}\begin{pmatrix} L & 2 & L' \\ 0 & -1 & 1 \end{pmatrix}$$
$$\times\left[\begin{pmatrix} L & 2 & L' \\ -K & -2 & (K+2) \end{pmatrix}\bar{C}_{K+2,1}{}^{L'}(6,7)+\begin{pmatrix} L & 2 & L' \\ -K & 2 & (K-2) \end{pmatrix}\bar{C}_{K-2,1}{}^{L'}(6,7)\right]=\delta_{L,0}\delta_{K,0}, \quad \text{(A3)}$$

$$(2L+1)^{-1}[(\omega-\omega_0+b)-i(T_2^{-1}+\tau_{L,K}^{-1})]\bar{C}_{K,1}{}^{L}(4,5)+(F_0+\tfrac{1}{2}D')\sum_{L'}\begin{pmatrix}L&2&L'\\-1&0&1\end{pmatrix}\begin{pmatrix}L&2&L'\\-K&0&K\end{pmatrix}\bar{C}_{K,1}{}^{L'}(4,5)$$

$$+(F_2+\tfrac{1}{2}D^{(2)\prime})\sum_{L'}\begin{pmatrix}L&2&L'\\-1&0&1\end{pmatrix}\left[\begin{pmatrix}L&2&L'\\-K&-2&(K+2)\end{pmatrix}\bar{C}_{K+2,1}{}^{L'}(4,5)+\begin{pmatrix}L&2&L'\\-K&2&(K-2)\end{pmatrix}\bar{C}_{K-2,1}{}^{L'}(4,5)\right]$$

$$+D\sqrt{2}\sum_{L'}\begin{pmatrix}L&2&L'\\-1&1&0\end{pmatrix}\begin{pmatrix}L&2&L'\\-K&0&K\end{pmatrix}[\bar{C}_{K,0}{}^{L'}(1)+\bar{C}_{K,0}{}^{L'}(2)]$$

$$+D^{(2)}\sqrt{2}\sum_{L'}\begin{pmatrix}L&2&L'\\-1&1&0\end{pmatrix}\left[\begin{pmatrix}L&2&L'\\-K&-2&(K+2)\end{pmatrix}[\bar{C}_{K+2,0}{}^{L'}(1)+\bar{C}_{K+2,0}{}^{L'}(2)]\right.$$

$$\left.+\begin{pmatrix}L&2&L'\\-K&2&(K-2)\end{pmatrix}[\bar{C}_{K-2,0}{}^{L'}(1)+\bar{C}_{K-2,0}{}^{L'}(2)]\right]-\tfrac{1}{2}(D\sqrt{2})\sum_{L'}\begin{pmatrix}L&2&L'\\-1&-1&2\end{pmatrix}\begin{pmatrix}L&2&L'\\-K&0&K\end{pmatrix}\bar{C}_{K,2}{}^{L'}(8,9)$$

$$-\tfrac{1}{2}(D^{(2)}\sqrt{2})\sum_{L'}\begin{pmatrix}L&2&L'\\-1&-1&2\end{pmatrix}\left[\begin{pmatrix}L&2&L'\\-K&-2&(K+2)\end{pmatrix}\bar{C}_{K+2,2}{}^{L'}(8,9)\right.$$

$$\left.+\begin{pmatrix}L&2&L'\\-K&2&(K-2)\end{pmatrix}\bar{C}_{K-2,2}{}^{L'}(8,9)\right]=0, \quad \text{(A4)}$$

$$(2L+1)^{-1}[(\omega-\omega_0-b)-i(T_2^{-1}+\tau_{L,K}^{-1})]\bar{C}_{K,1}{}^{L}(6,7)+(F_0-\tfrac{1}{2}D')\sum_{L'}\begin{pmatrix}L&2&L'\\-1&0&1\end{pmatrix}\begin{pmatrix}L&2&L'\\-K&0&K\end{pmatrix}$$

$$\times\bar{C}_{K,1}{}^{L'}(6,7)+(F_2-\tfrac{1}{2}D^{(2)\prime})\sum_{L'}\begin{pmatrix}L&2&L'\\-1&0&1\end{pmatrix}\left[\begin{pmatrix}L&2&L'\\-K&-2&(K+2)\end{pmatrix}\bar{C}_{K+2,1}{}^{L'}(6,7)+\begin{pmatrix}L&2&L'\\-K&2&(K+2)\end{pmatrix}\right.$$

$$\left.\times\bar{C}_{K-2,1}{}^{L'}(6,7)\right]+D\sqrt{2}\sum_{L'}\begin{pmatrix}L&2&L'\\-1&1&0\end{pmatrix}\begin{pmatrix}L&2&L'\\-K&0&K\end{pmatrix}[\bar{C}_{K,0}{}^{L'}(2)+\bar{C}_{K,0}{}^{L'}(3)]$$

$$+D^{(2)}\sqrt{2}\sum_{L'}\begin{pmatrix}L&2&L'\\-1&1&0\end{pmatrix}\left[\begin{pmatrix}L&2&L'\\-K&-2&(K+2)\end{pmatrix}[\bar{C}_{K+2,0}{}^{L'}(2)+\bar{C}_{K+2,0}{}^{L'}(3)]\right.$$

$$\left.+\begin{pmatrix}L&2&L'\\-K&2&(K-2)\end{pmatrix}[\bar{C}_{K-2,0}{}^{L'}(2)+\bar{C}_{K-2,0}{}^{L'}(3)]\right]-\tfrac{1}{2}(\sqrt{2}D)\sum_{L'}\begin{pmatrix}L&2&L'\\-1&-1&2\end{pmatrix}\begin{pmatrix}L&2&L'\\-K&0&K\end{pmatrix}\bar{C}_{K,2}{}^{L'}(8,9)$$

$$-\tfrac{1}{2}(D^{(2)}\sqrt{2})\sum_{L'}\begin{pmatrix}L&2&L'\\-1&-1&2\end{pmatrix}\left[\begin{pmatrix}L&2&L'\\-K&-2&(K+2)\end{pmatrix}\bar{C}_{K+2,2}{}^{L'}(8,9)\right.$$

$$\left.+\begin{pmatrix}L&2&L'\\-K&2&(K-2)\end{pmatrix}\bar{C}_{K-2,2}{}^{L'}(8,9)\right]=0, \quad \text{(A5)}$$

$$(2L+1)^{-1}[(\omega-\omega_0)-i(T_2^{-1}+\tau_{L,K}^{-1})]\bar{C}_{K,2}{}^{L'}(8,9)-F_0\sum_{L'}\begin{pmatrix} L & 2 & L' \\ -2 & 0 & 2\end{pmatrix}\begin{pmatrix} L & 2 & L' \\ -K & 0 & K\end{pmatrix}\bar{C}_{K,2}{}^{L'}(8,9)$$

$$-F_2\sum_{L'}\begin{pmatrix} L & 2 & L' \\ -2 & 0 & 2\end{pmatrix}\left[\begin{pmatrix} L & 2 & L' \\ -K & -2 & (K+2)\end{pmatrix}\bar{C}_{K+2,2}{}^{L'}(8,9)+\begin{pmatrix} L & 2 & L' \\ -K & 2 & (K-2)\end{pmatrix}\bar{C}_{K-2,2}{}^{L'}(8,9)\right]$$

$$-\tfrac{1}{2}(D\sqrt{2})\sum_{L'}\begin{pmatrix} L & 2 & L' \\ -2 & 1 & 1\end{pmatrix}\begin{pmatrix} L & 2 & L' \\ -K & 0 & K\end{pmatrix}[\bar{C}_{K,1}{}^{L'}(4,5)+\bar{C}_{K,1}{}^{L'}(6,7)]$$

$$-\tfrac{1}{2}(D^{(2)}\sqrt{2})\sum_{L'}\begin{pmatrix} L & 2 & L' \\ -2 & 1 & 1\end{pmatrix}\left[\begin{pmatrix} L & 2 & L' \\ -K & -2 & (K+2)\end{pmatrix}[\bar{C}_{K+2,1}{}^{L'}(4,5)+\bar{C}_{K+2,1}{}^{L'}(6,7)]\right.$$

$$\left.+\begin{pmatrix} L & 2 & L' \\ -K & 2 & (K-2)\end{pmatrix}[\bar{C}_{K-2,1}{}^{L'}(4,5)+\bar{C}_{K-2,1}{}^{L'}(6,7)]\right]=0, \quad \text{(A6)}$$

and the absorption Z'' is given by:

$$Z''=(1/3\pi)\,\mathrm{Im}[\bar{C}_{0,0}{}^{0}(1)+\bar{C}_{0,0}{}^{0}(2)+\bar{C}_{0,0}{}^{0}(3)]. \quad \text{(A7)}$$

Considerable simplification has been achieved by setting $\omega_n=0$, i.e., neglecting the nuclear Zeeman term. We have checked the simulations of Eqs. (A1)–(A7) with those for which $\omega_n/(|\gamma_e|)=0.36$ G and have found virtually no differences. It is also a common approximation made in analyzing X-band rigid spectra.[29]

One can relate the Eqs. (A1)–(A6) to the axially symmetric equations of I where ω_n was not set equal to zero by noting that the coefficients $\bar{C}_{K,M}{}^{L}$ in the above equations are defined as:

$$\bar{C}_{K,M}{}^{L}=\tfrac{1}{2}(C_{K,M}{}^{L}+C_{-K,M}{}^{L}), \qquad K\geq 0, \quad \text{(A8)}$$

$$\bar{C}_{K,M}{}^{L}(i,j)=\bar{C}_{K,M}{}^{L}(i)\mp\bar{C}_{K,-M}{}^{L}(j), \quad \text{(A9)}$$

where the minus sign is for $i=4, j=5$ and $i=6, j=7$, while the plus sign is for $i=8, j=9$.

Definitions of other terms in Eqs. (A1)–(A6) are:

$$F_0=(2/3)^{1/2}g^{(0)}\beta_e B_0\hbar^{-1},$$

$$F_2=(2/3)^{1/2}g^{(2)}\beta_e B_0\hbar^{-1},$$

$$D=-2\pi\xi_N D^{(0)},$$

$$D^{(2)}=-2\pi\xi_N D^{(\pm 2)},$$

$$D'=-(8/3)^{1/2}D,$$

$$D^{(2)\prime}=-(8/3)^{1/2}D^{(2)},$$

$$b=-\tfrac{1}{2}a_N|\gamma_e|,$$

where all terms are in angular frequency units of sec^{-1}.

The coupled equations (A1)–(A7) were solved either by Gaussian elimination or by a diagonalization of the appropriately symmetrized equations[4] on an IBM 360/65 computer using Fortran IV language. Programs are available upon request.

* Supported in part by the Advanced Research Projects Agency and by a grant from the National Science Foundation (Grant No. GP-13780).

† NDEA Title IV Fellow.

‡ National Institutes of Health Predoctoral Fellow.

[1] (a) W. L. Hubbell and H. M. McConnell, J. Am. Chem. Soc. **93,** 314 (1971). (b) H. M. McConnell and B. G. McFarland, Quart. Rev. Biophys. **3,** 91 (1970). (c) J. R. Norris and S. I. Weissman, J. Phys. Chem. **73,** 3119 (1969).

[2] J. H. Freed and G. K. Fraenkel, J. Chem. Phys. **39,** 326 (1963).

[3] D. Kivelson, J. Chem. Phys. **33,** 1094 (1960).

[4] J. H. Freed, G. V. Bruno, and C. F. Polnaszek, MSC Cornell University, Report # 1484, Nov. 1970; Abstracts, 2nd Symposium on ESR, Athens, Ga., Dec. 1970; J. Phys. Chem. **75,** 3385 (1971). References to this work are designated by I.

[5] M. S. Itzkowitz, J. Chem. Phys. **46,** 3048 (1967).

[6] (a) N. N. Korst and A. V. Lazarev, Mol. Phys. **17,** 481 (1969); (b) I. V. Alexandrov, A. N. Ivanova, N. N. Korst, A. V. Lazarev, A. I. Prikhozhenko, and V. B. Stryukov, Mol. Phys. **18,** 681 (1970).

[7] H. Sillescu, J. Chem. Phys. **54,** 2110 (1971).

[8] R. G. Kooser, W. V. Volland, and J. H. Freed, J. Chem. Phys. **50,** 5243 (1969).

[9] J. W. H. Schreurs and G. K. Fraenkel, J. Chem. Phys. **34,** 756 (1961).

[10] Z. Luz, B. L. Silver, and C. Eden, J. Chem. Phys. **44,** 4421 (1966).
[11] J. G. Powles and M. H. Mosley, Proc. Phys. Soc. (London) **77,** 729 (1961).
[12] D. Kivelson and G. Collins, *Proceedings of the 1st International Conference on Magnetic Resonance, Jerusalem, Israel, 1961* (Wiley, New York, 1962), p. 496.
[13] J. H. Freed, J. Chem. Phys. **41,** 2077 (1964).
[14] The E-12 spectrometer was obtained with the support of NSF Grant No. GP-10595.
[15] S. B. Wagner, M.S. thesis, Cornell University, Ithaca, N.Y. 14850.
[16] R. J. Faber and G. K. Fraenkel, J. Chem. Phys. **47,** 2462 (1967).
[17] "EPR at Work," Instrument Division of Varian Associates, No. 29.
[18] G. K. Fraenkel, J. Phys. Chem. **71,** 139 (1967).
[19] *Handbook of Chemistry and Physics*, edited by C. D. Hodgman (Chemical Rubber Publishing Co., Cleveland, Ohio, 1962), 43rd Ed.
[20] G. E. McDuffie, R. G. Quinn, and T. A. Litovitz, J. Chem. Phys. **37,** 239 (1962).
[21] J. S. Leigh, Jr. and G. H. Reed, J. Phys. Chem. **75,** 1202 (1971).
[22] It is possible that this "exchange-broadened" line results from the dimerization of PADS. Paramagnetism and a broad EPR signal at $g=2$ have been observed in some crystals of $K_4(PADS)_2$ (cf., W. Moser and R. A. Howie, J. Chem. Soc. A 1968, 3039).
[23] J. H. Freed and G. K. Fraenkel, J. Chem. Phys. **40,** 1815 (1964).
[24] For $T<-20°C$, the viscosity values used were obtained from extrapolating the $T=+100°C$ to $-20°C$ viscosity data. A best fit over this temperature range was obtained with $\log\eta \propto (4/T^3+1/T^4)$. It has been previously noted that the viscosity data could be described by $\log\eta \propto 1/T^3$ [cf., W. M. Slie, A. R. Donfor, Jr., and T. A. Litovitz, J. Chem. Phys. **44,** 3712 (1966)].
[25] G. K. Fraenkel, J. Chem. Phys. **42,** 4275 (1965).
[26] O. H. Griffith, D. W. Cornell, and H. M. McConnell, J. Chem. Phys. **43,** 2909 (1965).
[27] S. I. Weissman and D. Banfill, J. Am. Chem. Soc. **75,** 2534 (1953).
[28] The rigid spectra were simulated from the methods given by R. Lefebvre and J. Maruani, J. Chem. Phys. **42,** 1480 (1965).
[29] L. J. Libertini and O. H. Griffith, J. Chem. Phys. **53,** 1359 (1970).
[30] Some rigid limit simulations were performed with a Gaussian line shape. However, the agreement between simulated and observed spectra, for this choice of line shape, was inferior to that obtained with a Lorentzian line shape. It is possible that a combination of line shapes might yield better results, but this was not attempted.
[31] In Ref. 29 it was noted that the linewidth of DTBN varied from 1.4–2.7 G with orientation, but insufficient information was given to make a comparison between this variation and the observed variation for PADS.
[32] This indicates that the orientation dependence does not result from the unresolved intermolecular proton (deuterium) dipolar interactions between PADS and solvent molecules. If the 1 G difference in the residual linewidth of frozen H_2O and D_2O is attributed to the 6.5:1 ratio of the nuclear moments of ^1H and ^2D, the solvent contribution to the residual derivative linewidth is ~1.2 G and ~0.15 G, respectively. The remaining 0.9–1.3 G contribution to the linewidth might possibly be attributed to variations in A_i and g_i resulting from local differences in the crystal field and solvent interactions, but one would expect a better fit to a Gaussian than Lorentzian line shape.
[33] Libertini and Griffith (Ref. 29) note that the coordinate axes of the **A** and **g** tensors for DTBN do not exactly coincide and that there is a 6° difference in the xy plane. If this is true for PADS it could affect the accuracy of the simulated spectra. Since the **A** tensor, for PADS, is almost axially symmetric, differences in the xy plane would not be expected to have a large effect. However, any noncoincidence of the z axes would be significant.
[34] One can estimate that the quadrupole moment of a $2p$–π electron is about 5–8 MHz [cf., Ref. 23] and that for nitroxides the spin density $\rho_N \cong 0.5$ [cf., J. S. Hyde, C. W. Chien, and J. H. Freed, J. Chem. Phys. **48,** 4421 (1968)]. If a quadrupole moment of 4 MHz is assumed, the linewidth contributions from quadrupole relaxation can be estimated to be less than 0.4% of the dipolar terms.[2]
[35] R. Wilson and D. Kivelson, J. Chem. Phys. **44,** 154 (1966). If their expression for the linewidth variations is used, $\Delta H=\alpha+\beta M+\gamma M^2+\delta M^3$, approximate calculations show that for PADS: $\delta/B\approx 1\times10^{-3}$, $|\beta-B|/B\approx 5\times10^{-3}$, $|\gamma-C|/C\approx 4\times10^{-5}$.
[36] R. A. Howie, L. S. D. Glasser, and W. Moser, J. Chem. Soc. A **1968,** 3043.
[37] Note that as long as $R_{z'}\gg R_{x'}$, $R_{y'}$ one may satisfactorily treat the motion as being axially symmetric with $R_1=\frac{1}{2}(R_{x'}+R_{y'})$, cf., Ref. 13.
[38] P. W. Atkins and D. Kivelson, J. Chem. Phys. **44,** 169 (1966).
[39] P. W. Atkins, Mol. Phys. **12,** 133 (1967). The theory for anisotropic reorientation has not yet been fully resolved [P. W. Atkins (private communication)].
[40] The discrepancy between the observed and calculated values of A cannot be attributed to uncertainty in the value for N, since calculations employing Eq. (5) indicate that A is virtually independent of N.
[41] It is not difficult to include such orientation-dependent widths into the slow tumbling equations, but we have not done so.
[42] P. A. Egelstaff, J. Chem. Phys. **53,** 2590 (1970).
[43] E. N. Ivanov, Zh. Eksp. Teor. Fiz. **45,** 1509 (1963) [Sov. Phys. JETP **18,** 1041 (1964)].
[44] This form is still only a simplified but useful approximation, cf., R. A. Sack, Proc. Phys. Soc. (London) **70,** 402, 414 (1957) and Ref. 45.
[45] W. A. Steele, J. Chem. Phys. **38,** 2404, 2411 (1963). One can relate the equations of Steele to those given in Ref. 42 by letting $\tau=I/\xi$ where I is the moment of inertia and ξ the friction coefficient, thus $R=kT\xi$.
[45a] *Note added in proof*: ESR spectra of H. M. McConnell *et al.* (private communication) of spin-labeled hemoglobin in the slow tumbling region do show the distinctive features of Brownian diffusion as would be expected for this macromolecule.
[46] J. H. Freed, *NATO Summer School Lectures on ESR Relaxation in Liquids, Norway, 1971* (Plenum, New York, to be published).
[47] P. C. Martin and S. Yip, Phys. Rev. **170,** 151 (1968).
[48] L. Onsager and L. K. Runnels, J. Chem. Phys. **50,** 1089 (1969).